Title
THE MOLECULAR-BEAM ELECTRIC-RESONANCE SPECTRA OF LiF, NaF, AND KC1

Author
Hollowell, Craig D.

Publication Date
1966-11-07

UCRL-17019
Preprint

University of California

Ernest O. Lawrence Radiation Laboratory

THE MOLECULAR-BEAM ELECTRIC-RESONANCE SPECTRA OF LiF, NaF, and KCl

Berkeley, California

DISCLAIMER

UCRL-17019

UNIVERSITY OF CALIFORNIA

Lawrence Radiation Laboratory
Berkeley, California

AEC Contract No. W-7405-eng-48

THE MOLECULAR-BEAM ELECTRIC-RESONANCE SPECTRA OF LiF, NaF, AND KCl

Craig D. Hollowell

(Ph.D. Thesis)

November 7, 1966

THE MOLECULAR-BEAM ELECTRIC-RESONANCE SPECTRA OF LiF, NaF, AND KCl

Contents

THE MOLECULAR-BEAM ELECTRIC-RESONANCE SPECTRA OF LiF, NaF, AND KCl

Craig D. Hollowell

Lawrence Radiation Laboratory
University of California
Berkeley, California

November 7, 1966

ABSTRACT

Radio-frequency spectra have been observed in the low vibrational and rotational states of $^{6}Li^{19}F$, $^{7}Li^{19}F$, $^{23}Na^{19}F$, $^{39}K^{35}Cl$, and $^{39}K^{37}Cl$ by the molecular-beam electric resonance method. Microwave $J = 1 \rightarrow 0$ transitions have also been observed for $^{23}Na^{19}F$. Analysis of the spectra has made possible the determination of accurate dipole moments, rotational constants, and nuclear hyperfine interaction constants.

A polarizable ion model of the alkali halide molecules is presented. This model includes several effects, previously neglected, and successfully agrees with experimental data.

I. INTRODUCTION

Many improvements in molecular-beam electric-resonance spectroscopy have been developed since the first spectrometer was constructed in 1947 by H. K. Hughes.[1] Hughes observed radio-frequency Stark transitions in CsF. Carlson, Lee and Fabricand[2] first reported on a weak field electric-resonance experiment in which a rotational transition of microwave frequency was induced in a polar diatomic molecule, and this was later extended to the strong field case by Wharton et al.[3] Trischka[4,5,6] improved on Hughes' design and developed a high resolution spectrometer. Since then many subtle changes in design by other experimenters have further increased the resolution and versatility of the molecular-beam spectrometer.

The present work is a continuation of the radio-frequency and microwave studies of the alkali halide molecules using a high resolutuion electric-resonance spectrometer. The spectrometer used in the present experiments has demonstrated very good resolution, even at strong Stark fields. This has made possible an accurate determination of electric dipole moments, as well as rotational and hyperfine interaction constants. This thesis presents the electric-resonance studies of LiF, NaF, and KCl in which accurate dipole moments and other molecular constants are reported, many for the first time.

Several attempts have been made to correlate experimental dipole moments and other molecular constants with a simple semi-classical ionic model of the alkali halides, none with complete success. With the present results and other recently reported accurate dipole moments now available, re-examination of the model has been undertaken. This thesis therefore presents a polarizable ion model of the alkali halide molecules which includes several effects, previously neglected, and which successfully agrees with experimental data.

II. EXPERIMENTAL PROCEDURE

A. Introduction

In molecular-beam resonance experiments molecules effuse from an oven source and pass through interchamber slits into a main chamber as shown in the schematic diagram of a typical spectrometer (Fig. 1). In an electric-resonance experiment the beam passes through three electric fields in the main chamber and is then focussed or defocussed onto a detector.

In the present experiments two inhomogeneous A and B dipole electric fields act as $(J,\pm m_J)$ state selectors of the beam. J is the rotational quantum number and m_J is its projection on the direction of the electric field. An inhomogeneous electric field exerts a force on a molecule having a permanent electric dipole moment, μ. This force can be expressed as:

$$F = -\frac{\partial W}{\partial x} = -\frac{\partial W}{\partial E}\frac{\partial E}{\partial x} = \mu_e \frac{\partial E}{\partial x}$$

where W is the energy of the molecule, E is the electric field, and x is the direction of the field gradient. The effective dipole moment, μ_e, is a function of the energy of the molecule in an electric field. A plot (Fig. 2) of μ_e/μ versus λ (a dimensionless parameter equal to $\mu E/B$ where B is the rotational constant) iluustrates the $(J,\pm m_J)$ dependence of μ_e as a function of the electric field. The trajectory of the beam in a $(J,\pm m_J)$ state can be calculated from the known field gradient, $\partial E/\partial x$, and effective dipole moment, μ_e. With proper values of the A and B electric fields, the $(J,\pm m_J)$ states can be focussed onto the detector. The experiments reported here are of the "flop-in" type and require that molecules undergo a transition in order to reach the detector. Therefore resonances are observed as increases of the beam intensity at the detector. This is shown in Fig. 1 where $(1,\pm 1)_A \rightarrow (1,0)_B$ transitions are refocussed.

The homogeneous electric C field removes the degeneracy between $|m_J|$ states of a diatomic molecule and this splitting is known as the Stark effect. Transitions of the type $(J,m_J)\rightarrow(J,m_J\pm 1)$ are induced by

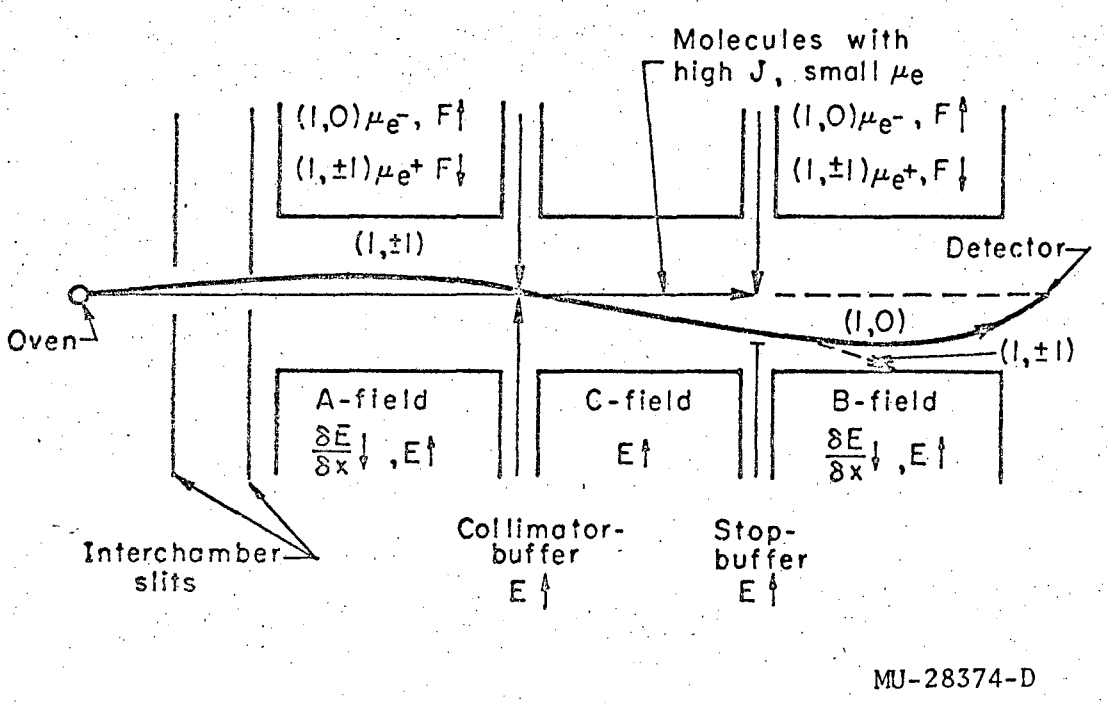

Fig. 1. A diagram of a typical molecular-beam electric-resonance spectrometer set up for doing "flop-in" experiments.

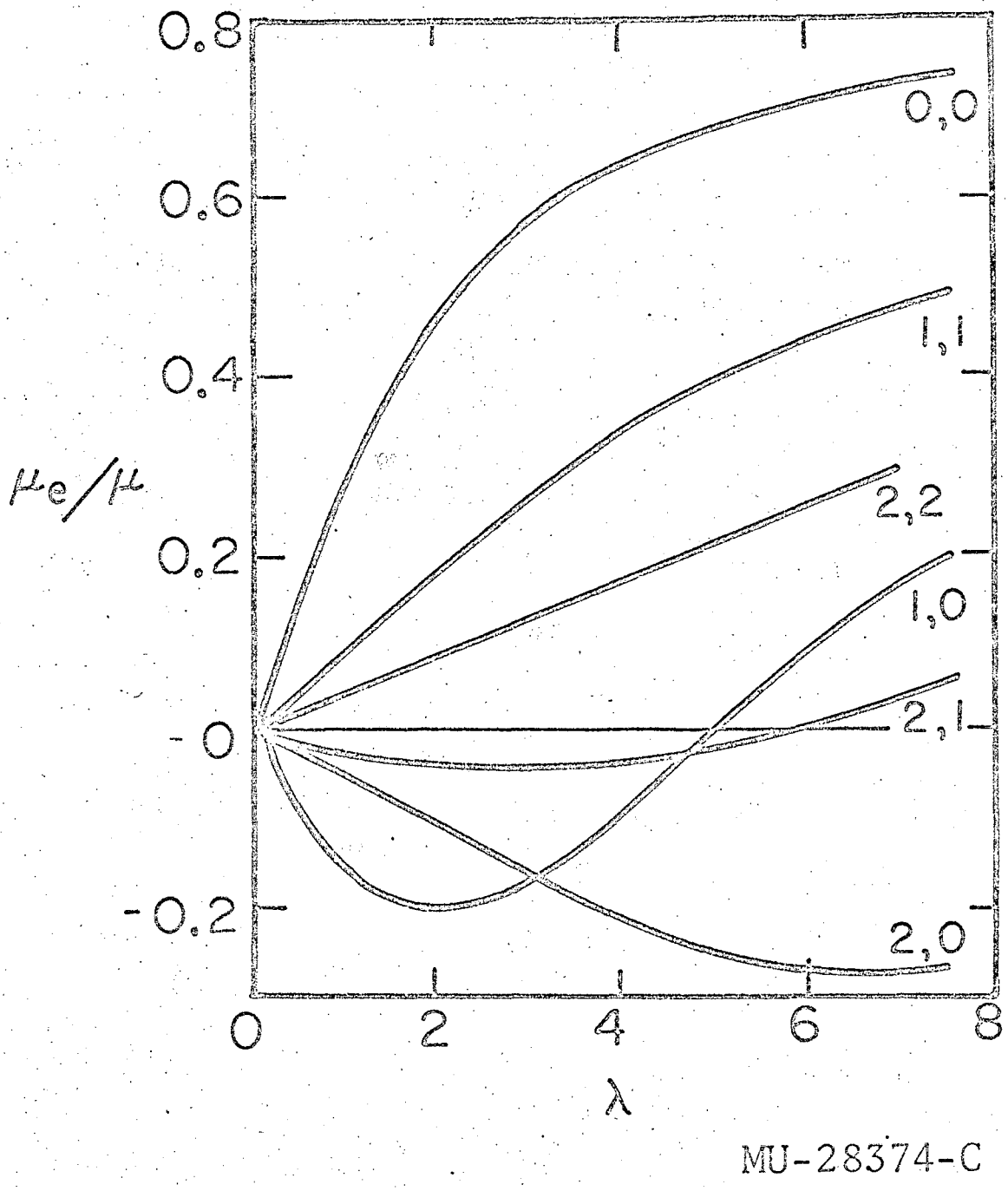

Fig. 2. The effective electric dipole moment, μ_e, for deflection of a diatomic molecule with a permanent dipole moment, μ. The numbers at the right of each curve represent the $(J,|m_J|)$ states. The dimensionless parameter λ is equal to $\mu E/B$ where E is the electric field and B is the rotational constant.

applying radio-frequency in the C field region of the apparatus. In the absence of any hyperfine structure, a single Stark transition resonance would be observed; however, the addition of hyperfine structure splits the $|m_J|$ levels and several resonances are observed.

Transitions between rotational J states can also be induced by applying microwave frequency and this is discussed further in Chapter IV.

B. The Spectrometer

The electric-resonance spectrometer used in these experiments was designed and constructed by A. J. Hebert.[7] Since the apparatus is discussed in detail in Hebert's thesis, only a brief description will be given here. The apparatus, shown schematically in Fig. 3, consists of a four-chamber high-vacuum system with two 30 cm. dipole inhomogeneous electric deflecting fields and a 30 cm homogeneous electric Stark field region. The Stark field is produced by parallel electrodes made by evaporating an aluminum film on glass optical flats. The field is parallel to 1/8 λ of helium light for a 1 cm gap or approximately 1 part in 10^5 along the 30 cm transition region. Radio-frequency is applied across one of the C field electrodes. Since magnetic effects could be expected to produce noticeable perturbations, care was taken to reduce all components of the earth's magnetic field and fringe magnetic fields from the mass spectrometer to less than 50 mg along the C field transition region.

The source oven is a 20% iridium - 80% platinum tube with a source slit 0.25 in. high by 0.005 in. wide. Detection is by surface ionization on a tungsten ribbon with the positive ions accelerated out of the main chamber, through a mass-analyzing magnet, and into a 14-stage electron multiplier.

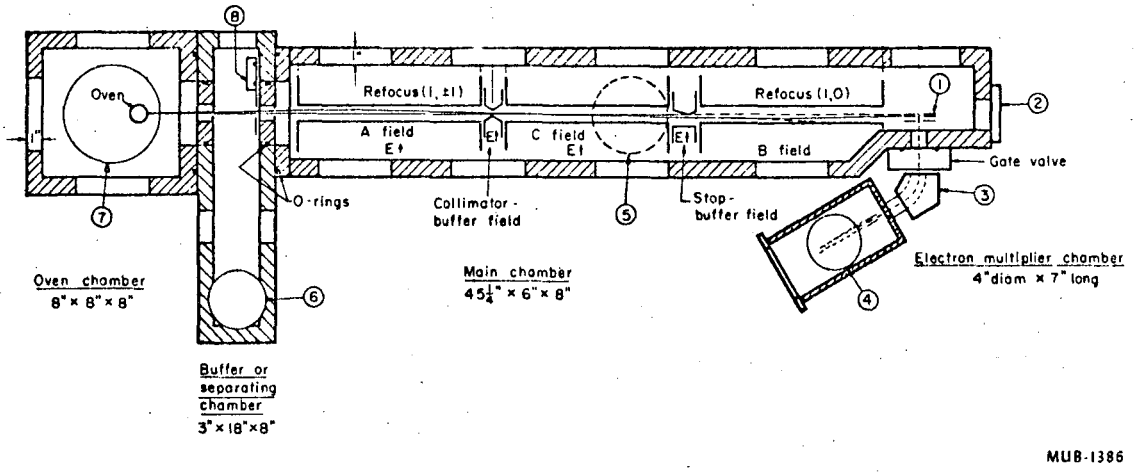

Fig. 3. Schematic diagram (top view) of the electric-resonance apparatus. Field lengths and displacements are to scale. Field gaps and beam displacements are exaggerated. Unshaded areas in chamber walls represent access ports.

(1) Hot wire and ion accelerator
(2) Glass cover port for optical alignment
(3) Permanent magnet, 60°, 1-cm gap
(4), (5), (6), and (7) Outlets to liquid nitrogen traps and oil diffusion pumps
(8) Gate valve and beam flag

C. Voltage Measurements

The value of the electric field is calculated from the known spacing of the homogeneous C field electrodes and the applied voltage. In early experiments the voltage was measured with a resistance bridge and a Rubicon potentiometer in conjunction with an Eppley standard cell. The uncertainty in electric field was 1 part in 10^4 with a reproducibility of the field at least an order of magnitude better.

However, an improved voltage measuring system now uses a Guildline Volt Ratio Box and a Leeds and Northrup Guarded Potentiometer which is calibrated with a bank of standard cells. The potentiometer and volt box have been certified by the National Bureau of Standards to 1 part in 10^6 and 1 part in 10^5, respectively. The cell bank is certified to 2 parts in 10^6. The spacing of the C field electrodes is corrected for thermal expansion by thermocouple monitoring of the three electrode spacers. This improved system has now reduced the electric field uncertainty to 2 parts in 10^5.

D. Radio-Frequency and Microwave Equipment

Hewlett-Packard 606A and 608C radio-frequency generators are used to produce signals from 50 kc/sec to 65 Mc/sec and from 10 Mc/sec to 480 Mc/sec, respectively. The radio-frequency signals are monitored with a H-P 5245L-5253A electronic counter. Pulses from the electron-multiplier, which are a direct measure of beam-intensity, are amplified and fed into a H-P 5245L-5253B counter. The radio-frequency count is fed into the first seven channels of a H-P 562A digital recorder and the beam-intensity is fed into the remaining four channels of the recorder. Also the first three digits of the beam-intensity count are converted into a voltage and fed into a Leeds and Northrup chart recorder for graphic representation of the spectrum. Radio-frequency is fed into the transition region at a fixed frequency and counted for 1 second while a 1-second beam intensity count is being taken. Both counts are recorded simultaneously, the frequency is increased and the counting cycle is restarted.

Microwave frequency is obtained by using a Hewlett-Packard 940A frequency doubler with the fundamental frequency generated by a "P-band" Varian X-12 klystron. The klystron is phase-locked with a H-P DY2650 A-M5 oscillator synchronizer to a H-P 608C signal generator. The fundamental frequency is monitored roughly with a wavemeter and more accurately with a H-P 540B transfer oscillator and a H-P 5245L-5253A frequency counter. Final frequency determinations are made with the 608C signal generator output. Microwave power is introduced into the electric field transition region means of a sectoral horn with a length of 14 in. and an apex of 20°.

III. THEORY

A. The Hamiltonian

The Hamiltonian for analyzing the electric-resonance spectrum of a polar diatomic molecule in a $^1\Sigma$ electronic ground state is:[8,9]

$$\mathcal{H} = B\underset{\sim}{J}^2 - \underset{\sim}{\mu}\cdot\underset{\sim}{E} - eq_1Q_1\frac{[3(\underset{\sim}{I}_1\cdot\underset{\sim}{J})^2 + \frac{3}{2}(\underset{\sim}{I}_1\cdot\underset{\sim}{J}) - (\underset{\sim}{I}_1^2\underset{\sim}{J}^2)]}{2I_1(2I_1-1)(2J-1)(2J+3)}$$

$$- eq_2Q_2\frac{[3(\underset{\sim}{I}_2\cdot\underset{\sim}{J})^2 + \frac{3}{2}(\underset{\sim}{I}_2\cdot\underset{\sim}{J}) - (\underset{\sim}{I}_2^2\underset{\sim}{J}^2)}{2I_2(2I_2-1)(2J-1)(2J+3)} + c_1(\underset{\sim}{I}_1\cdot\underset{\sim}{J}) + c_2(\underset{\sim}{I}_2\cdot\underset{\sim}{J})$$

$$+ c_3\frac{[3(\underset{\sim}{I}_1\cdot\underset{\sim}{J})(\underset{\sim}{I}_2\cdot\underset{\sim}{J}) + 3(\underset{\sim}{I}_2\cdot\underset{\sim}{J})(\underset{\sim}{I}_1\cdot\underset{\sim}{J}) - 2(\underset{\sim}{I}_1\cdot\underset{\sim}{I}_2)J(J+1)}{(2J-1)(2J+3)} + c_4(\underset{\sim}{I}_1\cdot\underset{\sim}{I}_2) \quad .$$

The first term in the above expression represents the rotation of the molecule, where B is the molecular rotational constant and $\underset{\sim}{J}$ is the rotational angular-momentum operator. The second term gives the interaction of the permanent electric dipole moment, $\underset{\sim}{\mu}$, with the applied external field, $\underset{\sim}{E}$. The third and fourth terms represent the interaction of the nuclear electric quadrupole moments (Q_1 and Q_2) with the electric field gradients at the nuclei (q_1 and q_2), where e is the electronic charge, I_1 and I_2 are the nuclear spins, and the subscripts distinquish between the two nuclei. The fifth and sixth terms represent the magnetic coupling of the nuclear spins with the molecular angular momentum, where c_1 and c_2 are the spin-rotation interaction constants The seventh and eighth terms represent the tensor and scalar spin-spin interactions,[10] respectively. The tensor spin-spin interaction constant, c_3, is defined as $c_3(\text{dir}) + c_3(\text{ind})$. The direct spin-spin interaction constant, $c_3(\text{dir})$, arises from the usual magnetic dipole-dipole interaction between the two nuclei, and equals $g_1g_2\mu_N^2\langle 1/r^3\rangle$ where g_1 and g_2 are the nuclear g factors for the two nuclei, r is the internuclear distance and μ_N is one nuclear magneton. For the $\langle 1/r^3\rangle$ calculation correction is made for the molecular vibrational effects as discussed by Ramsey.[11] The indirect spin-spin interaction constant, $c_3(\text{ind})$, arises from the tensor component of an electron-coupled nuclear spin-spin interaction. The scalar spin-spin interaction constant, c_4, arises soley from the scalar component of an electron-coupled nuclear spin-spin interaction.

B. Energy Calculations

A computer program[12] calculates the matrix elements of $\mathcal{H}$ in a $(J,I_1,I_2,m_J,m_{I_1},m_{I_2})$ representation, where m_J, m_{I_1}, and m_{I_2} are the projections of J,I_1, and I_2, respectively, on the the direction of the field E. The program computes the energy eigenvalues by diagonalizing this matrix and then claculates the spectral line positions and intensities corresponding to the given set of input parameters according to the selection rules $\Delta m_F = 0,\pm1,\pm2....$ where m_F is the projection of the total angular momentum on the field direction. Since m_F is a good quantum number at all field values, the matrix is diagonal in m_F. The unknown parameters are varied to obtain a best fit to the observed spectra.

The first term in the Hamiltonian is diagonal in J and the last four terms are small and only matrix elements diagonal in J are included for them.

The nonzero matrix elements of the Stark interaction are of the form $(J,m_J|\underset{\sim}{\mu}\cdot\underset{\sim}{E}|J\pm1,m_J)$. Since the matrix is infinite in J, only the first four J states are included in the matrix for $J = 1$ calculations, only the first five J states for $J = 2$ calculations and similarly for higher J state calculations. This is equivalent to a fourth-order perturbation treatment of the Stark energy.

The quadrupole terms have matrix elements diagonal in J as well as one connecting J with $J\pm2$. The quadrupole operator in the Hamiltonian given above can be used only to calculated matrix elements diagonal in J and therefore formulae derived by Fano[13] were used in calculating the off-diagonal matrix elements. This is equivalent to a second-order perturbation treatment of the quadrupole energy.

The line intensities are calculated from the matrix elements of the dipole moment operator using the computed wave functions.

IV. DATA ANALYSIS AND DISCUSSION OF THE ELECTRIC-RESONANCE SPECTRA OF SOME ALKALI HALIDE MOLECULES

A. The Radio-Frequency Spectra of $^{6}Li^{19}F$ and $^{7}Li^{19}F$

The radio-frequency Stark spectra of $^{6}Li^{19}F$ and $^{7}Li^{19}F$ were observed first by Trischka et al.[4,6,14] and more recently by Gold,[15] and by Wharton et al.[3,16] In the present work the resolution of the spectra is much better than previous experiments on LiF. The tables in this section compare the present work with that of Wharton et al.[3,16] The agreement is in general very good and indicates that a high degree of confidence can be placed in the dipole moments and hyperfine constants of LiF.

Radio-frequency transitions of the type $(J = 1, m_J = \pm 1) \rightarrow (J = 1, m_J = 0)$ and $(J = 2, m_J = \pm 2) \rightarrow (J = 2, m_J = \pm 1)$ were observed for the low vibrational states of LiF at several Stark field voltages. The observed full width at half maximum (FWHM) for lines in the J = 1 rotational state of $^{6}Li^{19}F$ was 3.5 kc/sec when approximately 1200 volts was applied to both state selecting A and B fields and 2.2 kc/sec when the fields were lowered to 600 volts. Typical spectra illustrating this effect are shown in Figs. 4 and 5. The effect is attributed to velocity selection by the deflecting fields, collimator, and stop system. With low voltages applied to the A and B fields, only those molecules which spend a longer time in the A and B field regions are deflected sufficiently to pass by the combination beam-stop buffer-field and reach the detector. Thus the low deflecting field spectra utilize molecules from the low velocity portion of the effusion spectrum These molecules spend more time in the C field transitions region and consequently give a smaller natural line width. This increased resolution, however, is gained only at the expense of intensity. Therefore the best spectra represent a compromise between line width and intensity. A spectrum of the type used in the $^{6}Li^{19}F$ analysis is shown in Fig. 4. The FWHM for $^{7}Li^{19}F$ spectra in the J = 1 rotational state was 4.0 kc/sec, and 3.0 kc/sec for the J = 2 spectra. Figures 6 and 7 show typical spectra for the J = 1 and 2 rotational states of $^{7}Li^{19}F$.

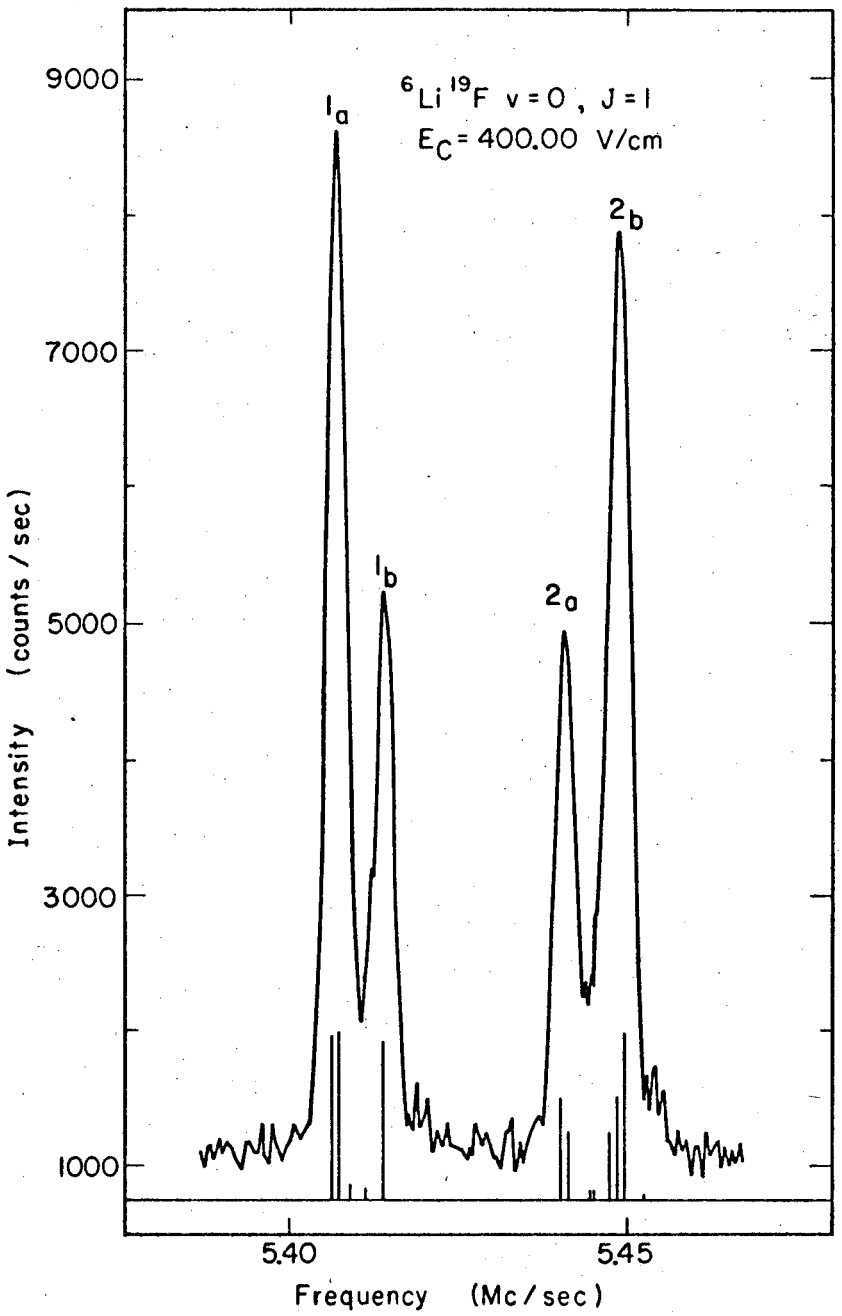

Fig. 4. A typical spectrum of $^6Li^{19}F$ with 1200 V applied to the deflecting fields. The thin vertical lines represent the calculated spectrum. FWHM = 3.5 kc/sec.

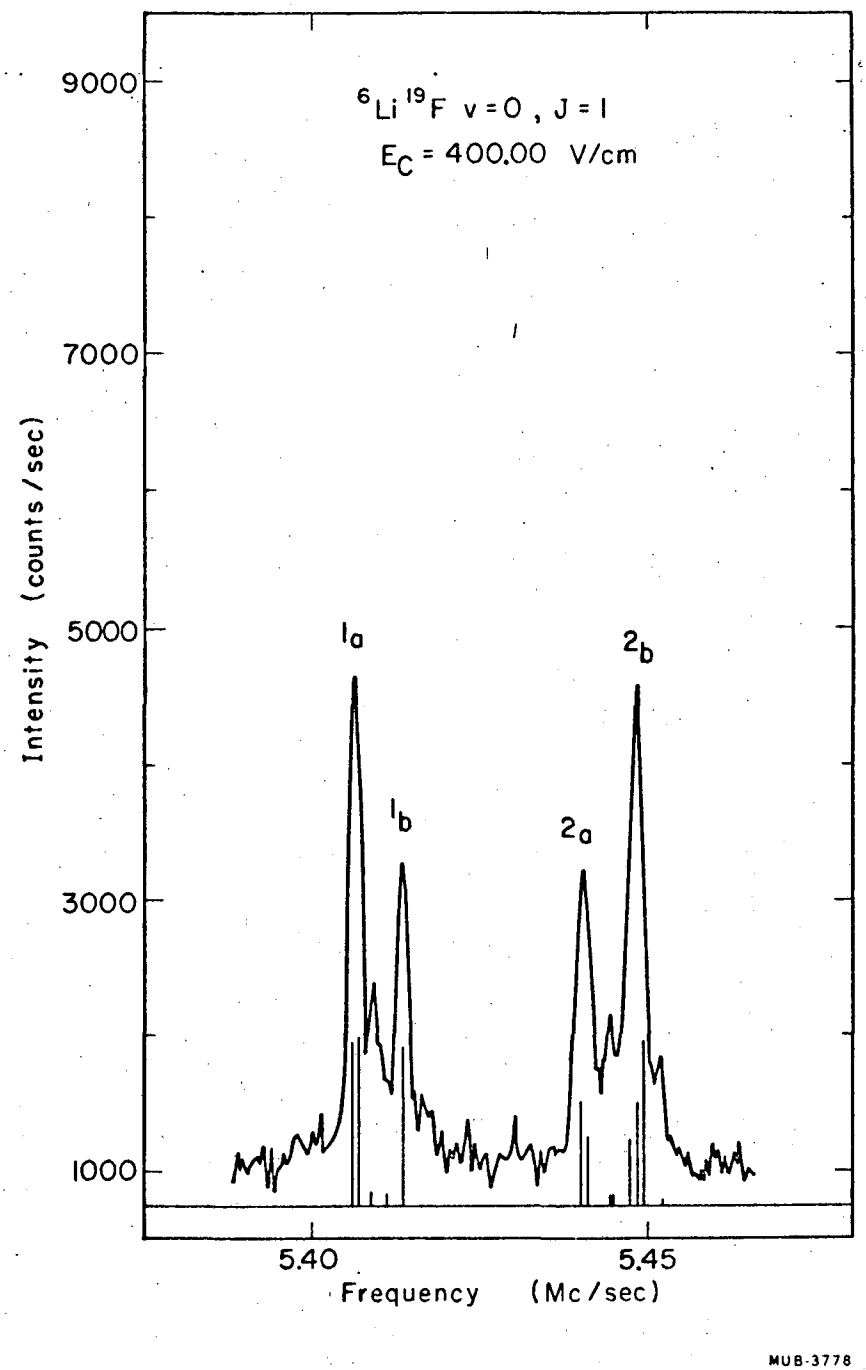

Fig. 5. A typical spectrum of $^6Li^{19}F$ with 600 V applied to the deflecting fields. The thin vertical lines represent the calculated spectrum. FWHM = 2.2 kc/sec.

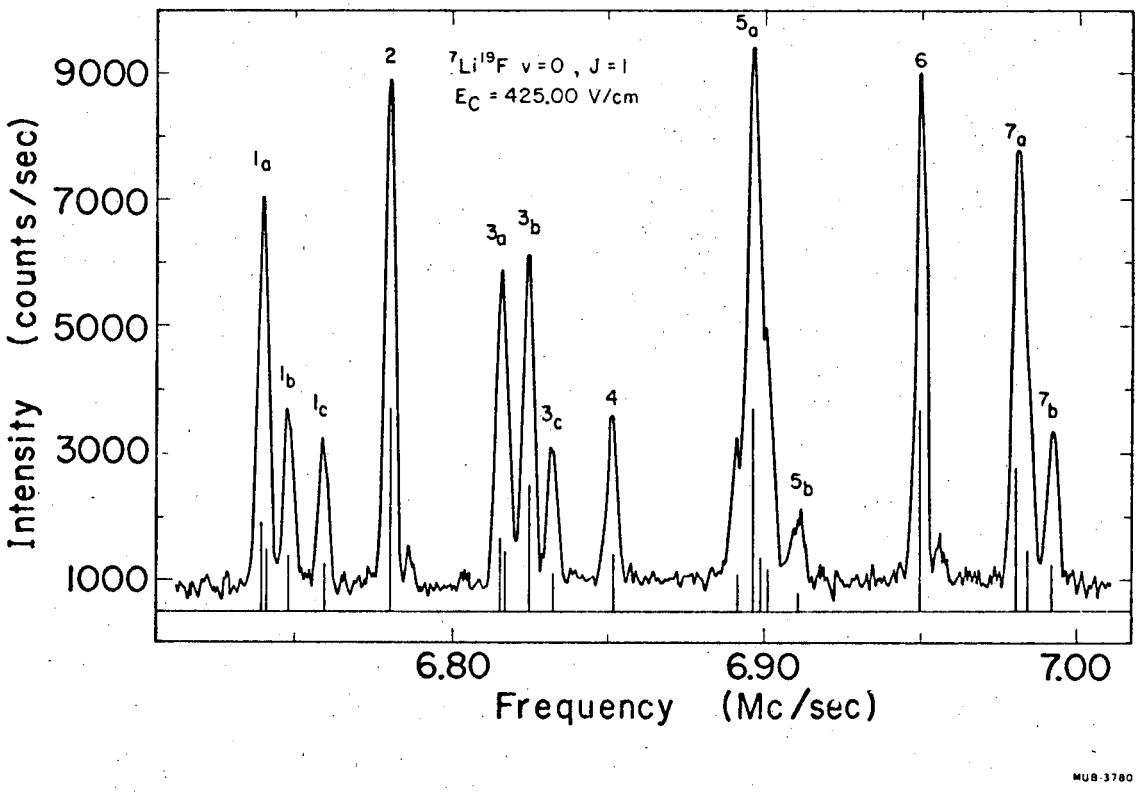

Fig. 6. A typical spectrum of $^7Li^{19}F$ for the v = 0, J = 1 state The thin vertical lines represent the calculated spectrum. FWHM = 4.0 kc/sec.

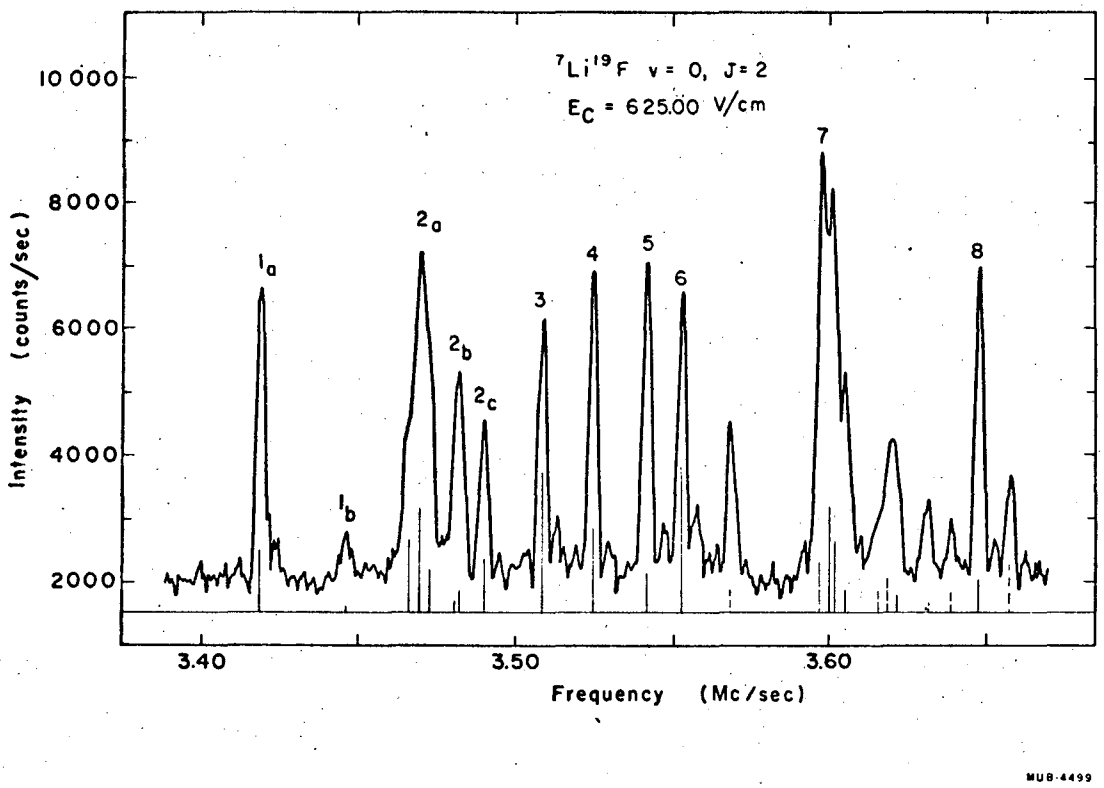

Fig. 7. A typical spectrum of $^7Li^{19}F$ for the v = 0, J = 2 state. The thin vertical lines represent the calculated spectrum. The dashed vertical lines to the right in the spectrum correspond to v = 1 peaks. The v = 1 spectral pattern is the same as that for v = 0 and it occurs at a slightly higher frequency. FWHM = 3.0 kc/sec.

The observed and calculated line positions used in the analysis of the spectra are given in Tables I, II, and III. The listed uncertainties in line positions are the experimentally observed average deviations. These uncertainties are in good agreement with the expected statistical uncertainties, and are ± 40 cps for the most intense $^{7}Li^{19}F$ J = 1 lines and ± 20 cps for a few J = 2 lines and the most intense lines observed in the $^{6}Li^{19}F$ spectra. Only resolved singlets were used to obtain best fits for the J = 1 spectra of $^{7}Li^{19}F$.

In the case of unresolved multiplets, calculated composite line positions were obtained by graphically adding component lines that had the experimental singlet line shape and calculated relative intensities. This technique was used to fit the spectra of $^{6}Li^{19}F$. The validity of the technique was checked by applying it to the unresolved multiplets in the v = 0, J = 1 spectrum of $^{7}Li^{19}F$ after obtaining a best fit with the singlets. The observed and predicted composite line positions are in excellent agreement as shown in Table II.

The J = 1 and J = 2 spectra of $^{7}Li^{19}F$ were fit independently. The agreement found between these two sets of results indicates a high degree of internal consistency. Excellent agreement was obtained between the calculated and observed LiF spectra for each of the vibrational and rotational states studied. In each case the average deviation of the fit is comparable to or better than the experimental average deviation.

The observed splitting for the low frequency doublet of $^{6}Li^{19}F$, (J = 1, v = 0), of 7.11 ± 0.06 kc/sec is somewhat larger than the value 6.91 ± 0.07 kc/sec reported by Wharton et al.[16] This splitting is important in the calculation of $(eqQ)_{6_{Li}}$.

The dipole moments were calculated from data taken at 800 V/cm and also at 1500 V/cm in the case of $^{6}Li^{19}F$. This latter experiment at 1500 V/cm utilized the improved voltage measuring system and was used as a check against the earlier dipole moment determinations. There is excellent agreement between both sets of dipole moments and good agreement with those of Wharton et al.[3] These results are summarized in Table IV.

Table I. Observed and calculated line positions for the J=1 radio-frequency spectra of $^{6}Li^{19}F$. All positions are given in kc/sec.

Line No.	Observed Line Positions	Calculated Line Positions	Calculated Relative Line Intensities	Final Calculated Composite Line Positions
		$(1, \pm1) \rightarrow (1,0)$, v = 0, E_C = 400 V/cm		
1_a	5406.64 ± 0.02	5406.20 5407.08	94 100	5406.64
1_b	5413.75 ± 0.04	5413.75	91	5413.75
2_a	5440.55 ± 0.05	5440.08 5441.25	52 41	5440.55
2_b	5448.74 ± 0.02	5447.40 5448.57 5449.44	40 58 94	5448.74
		$(1, \pm1) \rightarrow (1,0)$, v = 1, E_C = 400 V/cm		
1_a	5647.66 ± 0.02	5647.18 5648.14	35 37	5647.66
1_b	5654.69 ± 0.12	5654.69	33	5654.69
2_a	5680.96 ± 0.08	5680.47 5681.69	19 15	5680.96
2_b	5689.04 ± 0.02	5687.65 5688.87 5689.71	15 21 35	5689.04
		$(1, \pm1) \rightarrow (1,0)$, v = 2, E_C = 400 V/cm		
1_a	5899.02 ± 0.07	5898.86 5899.18	13 14	5899.02
1_b	5905.76 ± 0.25	5905.76	13	5905.76
2_a	5932.01 ± 0.13	5931.68 5932.48	7 6	5932.00
2_b	5939.66 ± 0.07	5938.70 5939.51 5940.24	6 8 13	5939.66

Table II. Observed and calculated line positions for the J=1 radio-frequency spectra of $^{7}Li^{19}F$. All positions are given in kc/sec.

Line No.	Observed Line Positions[a]	Calculated Line Positions	Differences	Calculated Relative Line Intensities
	$(1, \pm1)\rightarrow(1,0)$, $v = 0$, $E_C = 425$ V/cm			
1_a	(6739.60 ± 0.06)	(6739.53 ± 0.07)	+0.07	70
1_b	6748.27 ± 0.19	6748.17	+0.10	26
1_c	6759.57 ± 0.10	6759.58	-0.01	23
2	6780.42 ± 0.04	6780.38	+0.04	100
3_a	(6816.58 ± 0.07)	(6816.58 ± 0.07)	0.00	58
3_b	6825.05 ± 0.08	6824.97	+0.08	64
3_c	6832.83 ± 0.18	6832.69	+0.14	18
4	6851.90 ± 0.09	6852.08	-0.18	26
5_a	(6896.48 ± 0.06)	(6896.55 ± 0.12)	-0.07	103
6	6949.82 ± 0.04	6949.85	-0.03	100
7_a	(6980.72 ± 0.05)	(6980.52 ± 0.20)	+0.20	72
7_b	6991.84 ± 0.16	6991.69	+0.15	23
	$(1, \pm1)\rightarrow(1,0)$, $v = 1$, $E_C = 425$ V/cm			
1_b	7037.96 ± 0.25	7037.81	+0.15	10
1_c	7048.92 ± 0.12	7049.00	-0.08	8
2	7069.16 ± 0.03	7069.17	-0.01	37
3_b	7113.13 ± 0.18	7112.97	+0.16	23
3_c	7120.53 ± 0.16	7120.44	+0.09	7
4	7139.29 ± 0.15	7139.43	-0.14	10
6	7235.02 ± 0.03	7235.03	-0.01	37
7_b	7276.09 ± 0.33	7275.75	+0.24	8

Table II. (continued)

Line No.	Observed Line Positions[a]	Calculated Line Positions	Differences	Calculated Relative Line Intensities
	$(1, \pm 1) \rightarrow (1,0)$, $v = 2$, $E_c = 425$ V/cm			
1_b	7339.27 ± 0.11	7339.25	+0.02	4
1_c	7350.27 ± 0.17	7350.27	0.00	3
2	7369.53 ± 0.09	7369.58	-0.05	14
3_b	7413.00 ± 0.28	7412.83	+0.17	9
3_c	7419.85 ± 0.31	7419.90	-0.05	3
4	7438.50 ± 0.28	7438.47	+0.03	4
6	7531.89 ± 0.09	7531.84	+0.05	14
7_b	7571.45 ± 0.16	7571.42	+0.03	3

[a] The numbers in parentheses refer to unresolved multipletes and calculated composite lines. They were not used in obtaining a best fit and are listed here to illustrate the validity of the procedure used in fitting the $^6Li^{19}F$ spectra. The uncertainties given for the calculated composite positions are the estimated uncertainties in the line synthesis.

Table III. Observed and calculated line positions for the J=2 radio-frequency spectra of $^{7}Li^{19}F$. All positions are given in kc/sec.

Line No.	Observed Line Positions	Calculated Line Positions	Calculated Relative Line Intensities	Final Calculated Composite Line Positions	Differences
		$(2, \pm2) \rightarrow (2, \pm1)$, $v = 0$, $E_c = 625$ V/cm			
1	3418.82 ± 0.05	3418.74	42	3418.74	+0.08
2c	3490.33 ± 0.04	3490.38	35	3490.38	-0.05
3	3508.51 ± 0.02	3508.55	94	3508.55	-0.04
4	3424.53 ± 0.04	3524.50	55	3524.50	+0.03
5	3541.68 ± 0.05	3541.64 3541.84	26 26	3541.74	-0.06
6	3553.05 ± 0.02	3553.02	100	3553.02	+0.03
8	3647.53 ± 0.05	3647.41 3647.61	23 23	3647.51	+0.02
		$(2, \pm2) \rightarrow (2, \pm1)$, $v = 1$, $E_c = 625$ V/cm			
1	3568.79 ± 0.12	3568.85	15	3568.85	-0.06
3	3657.13 ± 0.03	3657.16	36	3657.16	-0.03
4	3672.21 ± 0.09	3672.25	20	3672.25	-0.04
5	3689.58 ± 0.05	3689.48 3689.67	10 10	3689.58	0.00
6	3700.19 ± 0.03	3700.17	37	3700.17	+0.02
8	3792.99 ± 0.14	3792.88 3793.07	8 8	3792.98	+0.01
		$(2, \pm2) \rightarrow (2, \pm1)$, $v = 2$, $E_c = 625$ V/cm			
1	3724.98 ± 0.10	3724.88	6	3724.88	+0.10
3	3811.80 ± 0.01	3811.79	13	3811.79	+0.01
4	3826.01 ± 0.02	3825.95	7	3825.95	+0.06
5	3843.32 ± 0.08	3843.32 3843.49	4 4	3843.40	-0.08
6	3853.32 ± 0.01	3853.33	14	3853.33	-0.01
8	3944.56 ± 0.09	3944.38 3944.56	3 3	3944.47	+0.09

Table IV. Dipole moments for LiF. All values are given in Debyes.

	Present results[a] (800 V/cm)	Present results[a] (1500 V/cm)	Wharton et al.[3]
		$^6Li^{19}F$	
μ_0	6.32736 ± 0.001	6.32753 ± 0.0002	6.32764 ± 0.001
μ_1	6.41473 ± 0.001	6.41489 ± 0.0002	6.41511 ± 0.001
μ_2	6.50317 ± 0.001	6.50334 ± 0.0002	6.50341 ± 0.001
μ_3	6.59273 ± 0.001		6.59326 ± 0.001
μ_e	6.28408 ± 0.0012	6.28426 ± 0.00025	6.38446 ± 0.001
μ_I	0.08630 ± 0.00021	0.08627 ± 0.00005	0.08612 ± 0.00003
μ_{II}	0.00053_5 ± 0.00008	0.00054_5 ± 0.00002	0.00060 ± 0.00002
		$^7Li^{19}F$	
μ_0	6.32481 ± 0.001		
μ_1	6.40723 ± 0.001		
μ_2	6.49054 ± 0.001		
μ_e	6.28393 ± 0.0012		
μ_I	0.08153 ± 0.00030		
μ_{II}	0.00044_5 ± 0.00012		

[a] The accuracy of the dipole moments is limited by the uncertainty in the absolute value of the electric Stark field; however, the precision of the results is at least an order of magnitude better and allows smaller errors to be reported for the coefficients in the dipole moment expressions.

The Stark effect interaction given in the Hamiltonian assumes a rigid rotor configuration and neglects the effect of the vibration-rotation interaction. This centrifugal distortion term is:[17]

$$W_{c.d.} = \frac{\mu_v^2 E^2}{hB_v}\left[- \frac{D_v}{B_v}\left(1 + \frac{1}{\theta_s}\right)\frac{J^2 + J + m_J^2 - 1}{(2J + 3)(2J - 1)}\right]$$

where the dipole derivative parameter, $1/\theta_s$, equals:

$$r_e/\mu_e \left(\partial\mu/\partial_r\right)_e$$

This effect is important for strong Stark field measurements and has been included in the LiF calculations. For the J = 1 rotational state of $^6Li^{19}F$, $W_{c.d.}$ is - 0.2 kc/sec at E_C = 800 V/cm and - 2.8 kc/sec at E_C = 1500 V/cm.

The observed dipole moments for the two isotopic species of LiF can be fitted to an expression of the form:

$$\mu_v = \mu_e + \mu_I (v + 1/2) + \mu_{II} (v + 1/2)^2$$

The equilibrium dipole moments, μ_e, are the same within experimental error, for $^6Li^{19}F$ and $^7Li^{19}F$. The coefficients μ_I and μ_{II} follow the isotopic dependence as predicted by theory. These quadratic expression coefficients are also given in Table IV.

The $^7Li^{19}F$ quadrupole coupling constants were fitted to a quadratic expression, however, the magnitude of the coefficient of the quadratic term is well below experimental error and probably is not significant. The quadrupole coupling constants for both LiF isotopes are summarized in Table V.

When corrected to a common vibrational energy, the ratio of the quadrupole coupling constants is:

$$[(eqQ)_e]_{^6Li} \Big/ [(eqQ)_e]_{^7Li} = 0.0205 \pm 0.002$$

Table V. Lithium quadrupole coupling constants for LiF. All values are given in kc/sec.

	Present results			Wharton et al.[16]
		$^{6}Li^{19}F$		
	J=1			J=1
$(eqQ)_0$	8.5 ± 0.8			7.3 ± 0.4
$(eqQ)_1$	8.6 ± 1.2			
$(eqQ)_2$	7.1 ± 2.0			
		$^{7}Li^{19}F$		
	J=1	J=2	Average[a]	J=1 and 2
$(eqQ)_0$	415.5 ± 0.4	415.7 ± 0.5	415.6 ± 0.4	416.02 ± 0.6
$(eqQ)_1$	406.0 ± 0.8	406.2 ± 0.8	406.1 ± 0.6	
$(eqQ)_2$	395.7 ± 1.2	396.8 ± 0.8	396.5 ± 0.8	
$(eqQ)_e$			420.3 ± 0.8	
$(eqQ)_I$			- 9.4 ± 1.2	
$(eqQ)_{II}$			-0.0_5 ± 0.9	

$$(eqQ)_v = (eqQ)_e + (eqQ)_I(v + 1/2) + (eqQ)_{II}(v + 1/2)^2$$

[a] Least squares average of J=1 and J=2 constants.

This value is in agreement with the ratio of nuclear quadrupole moments reported by Cranna,[18] $Q_{^6Li}/Q_{^7Li} = 0.019 \pm 0.001$; the value 0.023 ± 0.002 reported by Schuster and Pake;[19] and the value 0.0176 ± 0.001 of Wharton et al.[16]

The spin-rotation interaction arises from the magnetic coupling of the nuclear magnetic moments with the magnetic field of the rotating molecule. The spin-rotation interaction constant can be expressed as directly proportional to $\mu_N g_n B$[20] where μ_N is one nuclear magneton, g_n is the nuclear g factor and B is the rotational constant. The lithium and fluorine spin-rotation constants both agree with the calculated isotope ratios. The spin-rotation constants are given in Tables VI and VII. The differences between the J = 1 and J = 2 values reported for $c_{^7Li}$ are at the limit of the combined experimental errors and may not be significant.

Best fits to the observed spectra of $^7Li^{19}F$ were obtained by setting c_4 equal to zero and c_3 equal to the calculated $c_3(dir)$. The fits obtained for the J = 1 spectra and especially those obtained for the J = 2 spectra of $^7Li^{19}F$ indicate there is no justification for the inclusion of c_4 in these calculations or for assigning any value other than $c_3(dir)$ to c_3. In this respect the present results differ from those of Wharton et al.[16] and are compared in Table VIII. In all $^6Li^{19}F$ calculations $c_3(dir)$ was used for c_3, and c_4 is assumed to equal zero.

B. The Radio-Frequency and Microwave Spectra of $^{23}Na^{19}F$

Recent electric-resonance studies[21,22,23] of NaF have now been reported and serve as a comparision with the present work.[24] Earlier radio-frequency spectra by the magnetic-resonance method[25,26] had given somewhat less accurate values for the sodium quadrupole coupling constants than those now reported by the electric-resonance method.

Radio-frequency transitions of the type $(1, \pm1) \rightarrow (1,0)$ and $(2, \pm2) \rightarrow (2, \pm1)$ were observed for the low vibrational states of NaF. For the J = 1 rotational state, the spectrum consisted of six major line groups with hyper-

Table VI. Lithium spin-rotation interaction constants, c_{Li}, for LiF. All values are given in kc/sec.

Vibrational state	Present results			Wharton et al.[16]
	- - - $^{6}Li^{19}F$ - - -			
	J=1			
0	0.71 ± 0.08			
1	0.71 ± 0.12			
2	0.73 ± 0.20			
	- - - $^{7}Li^{19}F$ - - -			
	J=1	J=2	Average[a]	J=1 and 2
0	1.81 ± 0.06	1.89 ± 0.03	1.87 ± 0.03	1.80 ± 0.03
1	1.78 ± 0.08	1.85 ± 0.04	1.84 ± 0.04	
2	1.75 ± 0.10	1.80 ± 0.04	1.79 ± 0.04	

[a]Least squares average of J=1 and J=2 constants.

Table VII. Fluorine spin-rotation interaction constants, c_F, for LiF. All values are given in kc/sec.

Vibrational State	Present results			Wharton et al.[16]
		$^6Li^{19}F$		
		J=1		
0		36.75 ± 0.4		
1		36.08 ± 0.5		
2		35.66 ± 0.7		
		$^7Li^{19}F$		
	J=1	J=2	Average[a]	J=1 and 2
0	32.75 ± 0.3	32.65 ± 0.2	32.68 ± 0.16	32.37 ± 0.3
1	32.20 ± 0.3	32.20 ± 0.3	32.20 ± 0.22	
2	31.90 ± 0.4	31.80 ± 0.3	31.84 ± 0.24	

[a] Least squares average of J=1 and J=2 constants.

Table VIII. Spin-spin interaction constants, c_3 and c_4, for LiF. All values are given in kc/sec.

Vibrational state	c_3 Present results[a]	c_3 Wharton et al.[16]	c_4 Present results[a]	c_4 Wharton et al.[16]
		- - - $^6Li^{19}F$ - - - -		
	J=1		J=1	
0	4.307 ± 0.08		0.00 ± 0.15	
1	4.224 ± 0.12		0.00 ± 0.20	
2	4.140 ± 0.20		0.00 ± 0.40	
		- - - $^7Li^{19}F$ - - - -		
	J=1 and 2	J=1 and 2	J=1 and 2	J=1 and 2
0	11.382 ± 0.020	11.390 ± 0.015	0.00 ± 0.08	0.21 ± 0.04
1	11.173 ± 0.030		0.00 ± 0.11	
2	10.964 ± 0.030		0.00 ± 0.14	

[a] Best fits were obtained using the calculated c_3(dir) for the value of c_3. Thus in the present results, $c_3 = c_3$(dir). The uncertainties refer to the deviations which c_3 and c_4 may make while obtaining a fit to the data.

fine splittings resolvable in five of the six groups. Figure 8 shows the $v = 0$, $J = 1$ spectrum of NaF at a Stark field of 250 V/cm. The observed full width at half maximum intensity for resolved singlets was approximately 3 kc/sec, in agreement with the theoretical uncertainty line broadening. The signal-to-noise ratio was approximately 20 to 1 for observed transitions of the $v = 0$ vibrational state. Also shown in Fig. 8 are the calculated line positions and their relative intensities.

Figure 9 shows the $v = 0$, $J = 1$ and 2 energy levels of NaF, with respect to the Stark field strength, and the observed six major radio-frequency transitions in the absence of spin-rotation and spin-spin hyperfine structure.

The $J = 1 \rightarrow J = 0$ microwave transitions were observed by setting the Stark field and radio-frequency to give a maximum signal for a prominent line in the reorientation spectrum, i.e. a $J = 1$, $m_J = \pm 1 \rightarrow J = 1$, $m_J = 0$ transition. The microwave frequency was then swept and resonant frequency observed as a decrease in the radio-frequency "flop-in" signal due to depletion of the final state by a rotational transition of the type $J = 1$, $m_J = 0 \rightarrow J = 0$, $m_J = 0$. The decrease amounted to more than a 40% reduction in the "flop-in" Stark signal. The microwave line widths at half maximum were approximately 30 kc/sec.

Figure 9 shows the two major microwave transitions that could be observed for NaF using the above technique. Transitions labelled type II were observed for the first three vibrational states at a Stark field of 50 V/cm and both type I and II transitions were observed for these vibrational states at a field of 400 V/cm.

Table IX lists the observed and calculated line positions of NaF for the $J = 1$ and $J = 2$ rotational states. In the case of unresolved multiplets, calculated composite line positions were obtained by graphically adding component lines that had the experimental singlet line shapes and calculated relative intensities.

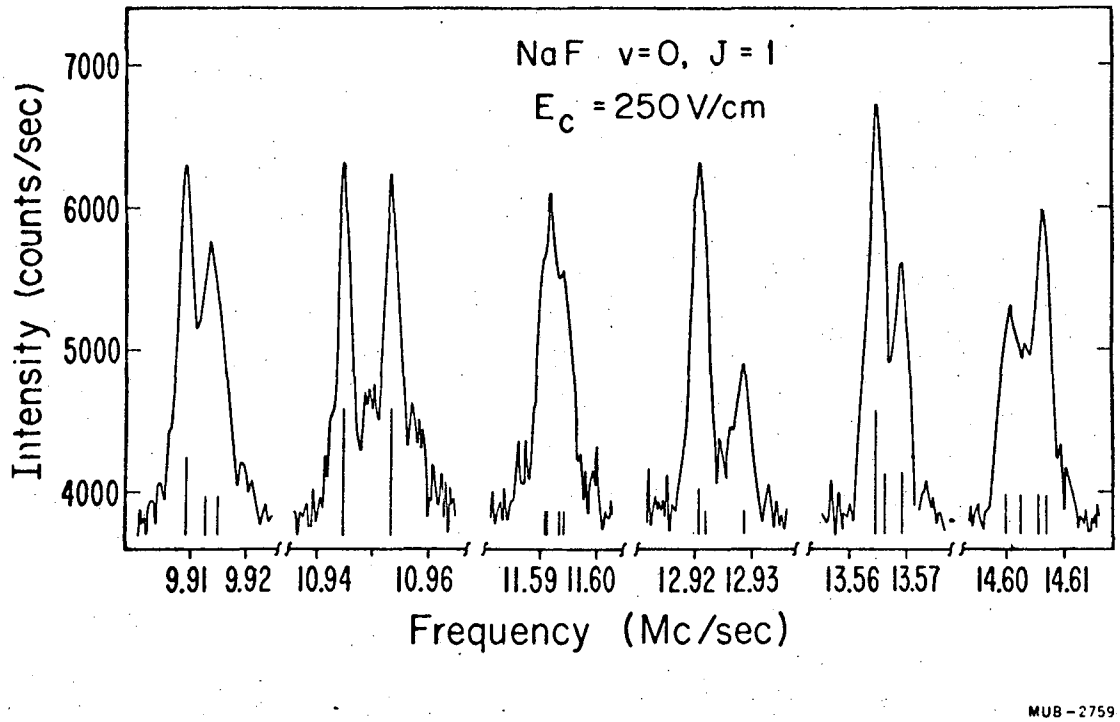

Fig. 8. A typical radio-frequency spectrum of $^{23}Na^{19}F$ in the v = 0 vibrational state. Transitions of the type $(1, \pm 1) \rightarrow (1,0)$ were observed at an electric field strength of 250 V/cm.

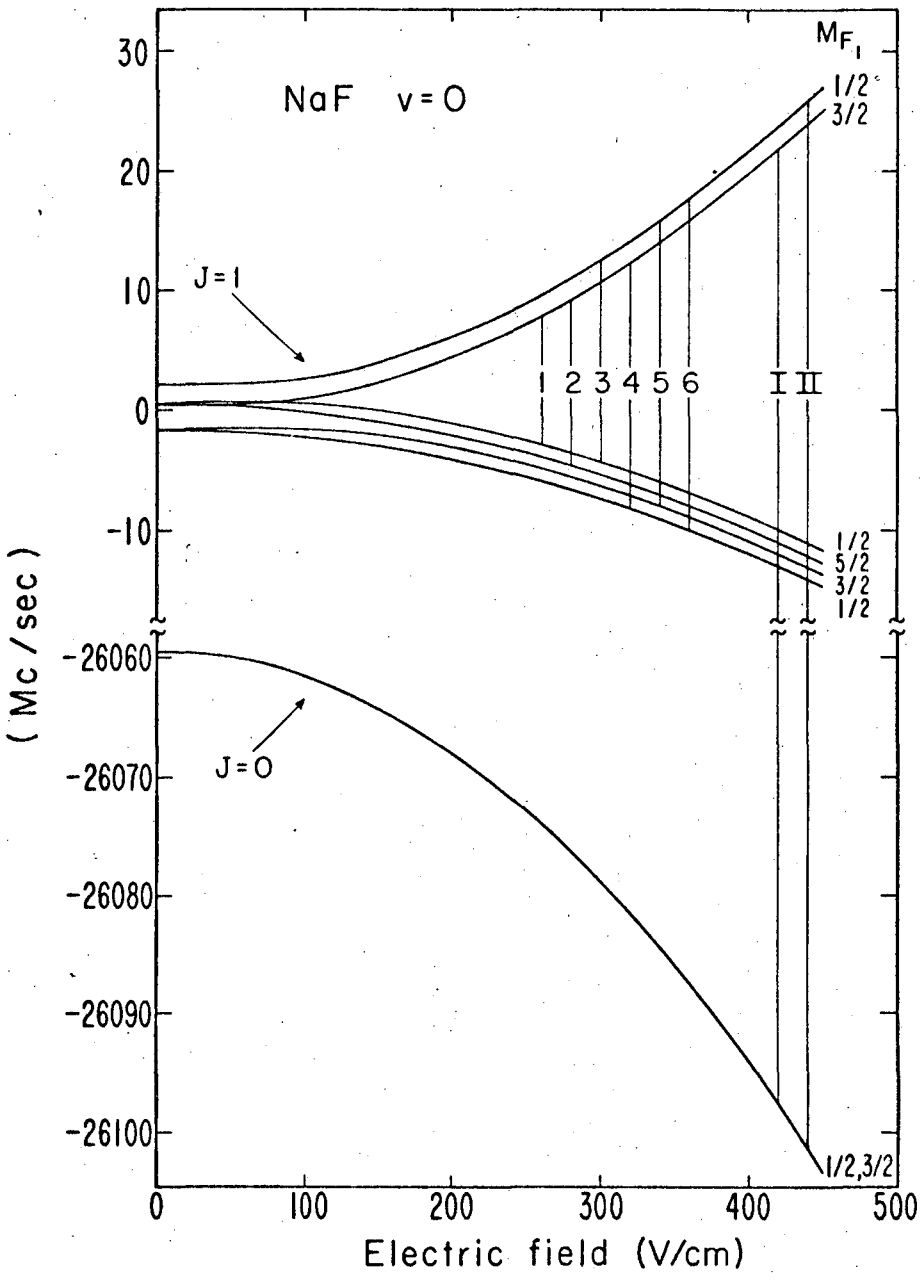

Fig. 9. The energy levels of $^{23}Na^{19}F$ with respect to the electric field strength. Arabic numerals refer to observed radio-frequency transitions and Roman numerals refer to microwave transitions. $M_{F_1} = m_J + m_{I_{Na}}$.

Table IX. Observed and calculated line positions for the radio-frequency spectra of $^{23}Na\ ^{19}F$

Line No.	Observed Line Positions (kc/sec)	Calculated Line Positions (kc/sec)	Calculated Relative Line Intensities	Final Calculated Composite Line Positions (kc/sec)
		$(1, \pm1) \rightarrow (1,0)$, $v = 0$, $E_C = 250$ V/cm		
1_a	9909.39 ± .17	9909.30	61	9909.30
1_b	9913.97 ± .24	9912.84	31	9913.98
		9915.12	31	
2_a	10945.08 ± .11	10945.04	100	10945.04
2_b	10953.47 ± .11	10953.42	100	10953.42
3	11592.12 ± .30	11591.02	18	11592.42
		11591.15	18	
		11593.31	18	
		11594.19	18	
4_a	12921.04 ± .09	12920.77	37	12921.04
		12921.84	18	
4_b	12928.55 ± .29	12928.84	18	12928.84
5_a	13564.69 ± .14	13564.39	98	13564.84
		13566.21	49	
5_b	13569.44 ± .38	13569.24	49	13569.24
6_a	14601.13 ± .35	14600.03	32	14601.33
		14602.63	31	
6_b	14606.48 ± .13	14605.66	32	14606.35
		14607.03	32	

Table IX (continued)

Line No.	Observed Line Positions(kc/sec)	Calculated Line Positions(kc/sec)	Calculated Relative Line Intensities	Final Calculated Composite Line Positions (kc/sec)
		$(1, \pm1) \rightarrow (1,0)$, v = 1, E_c = 250 V/cm		
1_a	10256.39 ± .17	10256.34	23	10256.34
1_b	10260.78 ± .30	10259.89	11	10261.03
		10262.17	11	
2_a	11280.32 ± .14	11280.40	37	11280.40
2_b	11288.85 ± .14	11288.85	37	11288.85
3	11917.19 ± .27	11915.98	7	11917.39
		11916.13	7	
		11918.26	7	
		11919.17	7	
4_a	13229.51 ± .11	13229.19	14	13229.47
		13230.30	7	
4_b	13237.27 ± .20	13237.30	7	13237.30
5_a	13862.36 ± .14	13861.75	36	13862.23
		13863.65	18	
5_b	13866.77 ± .27	13866.68	18	13866.68
6_a	14887.71 ± .12	14886.39	12	14887.69
		14888.98	12	
6_b	14892.75 ± .17	14892.02	12	14892.71
		14893.39	12	

Table IX (continued)

Line No.	Observed Line Positions(kc/sec)	Calculated Line Positions(kc/sec)	Calculated Relative Line Intensities	Final Calculated Composite Line Positions (kc/sec)
		$(1, \pm1) \rightarrow (1,0)$, $v = 2$, $E_c = 250$ V/cm		
1_a	10611.71 ± .32	10611.60	9	10611.60
1_b	10616.08 ± .37	10615.14	4	10616.26
		10617.38	4	
2_a	11625.03 ± .19	11625.08	14	11625.08
2_b	11633.55 ± .20	11633.42	14	11633.42
3	12251.75 ± .40	12250.20	3	12251.59
		12250.35	3	
		12252.44	3	
		12253.35	3	
4_a	13547.85 ± .16	13547.43	6	13547.71
		13548.56	3	
5_a	14170.18 ± .23	14169.90	14	14170.37
		14171.79	7	
6_b	15189.79 ± .23	15189.18	5	15189.86
		15190.54	5	
		$(2, \pm2) \rightarrow (2, \pm1)$, $v = 0$, $E_c = 500$ V/cm		
2_a	10734.62 ± .08	10734.70	100	10734.70
2_b	10740.86 ± .08	10740.86	100	10740.86
3_a	11134.86 ± .24	11134.89	32	11134.89
3_b	11139.07 ± .29	11138.74	14	11139.21
		11139.69	14	
5_a	12484.89 ± .15	12484.90	95	12484.90
5_b	12488.27 ± .21	12488.26	95	12488.26

The dipole moments for the first three vibrational states and the coefficients of the quadratic dipole expression are given in Table X. The dipole moments are significantly lower than those given by Bauer and Lew,[21] but agree with those reported by Gräff and Werth.[22]

The quadrupole coupling constants have also been fitted to an expression quadratic in vibrational number. The quadrupole coupling constants for the first three vibrational states and the terms of the quadratic expression are given in Table XI. The coefficient of the quadratic term is required for a best fit, although it is just at the limit of the experimental error and may not be significant.

The sodium and fluorine spin-rotation interaction constants did not show any significant change with vibrational state and are given as:

$$c_{Na} = 1.4 \pm 0.5 \text{ kc/sec}$$

$$c_{F} = 2.0 \pm 0.3 \text{ kc/sec}$$

In a first attempt to obtain a good fit between the observed and calculated line positions, the calculated value of $c_3(\text{dir})$ was used as the input for c_3 and only the parameters μ_v, $(eqQ)_v$, c_{Na}, c_F, and c_4 were varied. However, a good fit could not be found until c_3 was also varied. The experimentally determined value of c_3 is 3.85 ± 0.25 kc/sec, while $c_3(\text{dir})$ is calculated to be 4.157, 4.101, and 4.046 kc/sec for the $v = 0$, 1, and 2 vibrational states, respectively. No significant change with vibrational state was observed for c_3. The difference between $c_3(\text{dir})$ could be attributed to an indirect spin-spin interaction contribution, $c_3(\text{ind})$. Because of error limitations, however, this may not be significant.

Calculations indicate that c_4 can not be reliably determined with the present line widths (~3 kc/sec) and line position accuracies (~200 cps). However, an upper and lower limit of + 400 cps and - 100 cps, respectively, can be placed on this quantity.

Table X. Dipole moments for $^{23}Na^{19}F$

$\mu_0 = 8.15576 \pm 0.001$ D[a]	$\mu_e = 8.12349 \pm 0.0015$ D
$\mu_1 = 8.22086 \pm 0.001$ D	$\mu_I = 0.06436 \pm 0.0008$ D
$\mu_2 = 8.28670 \pm 0.001$ D	$\mu_{II} = 0.00037 \pm 0.0003$ D

$$\mu_v = \mu_e + \mu_I (v + 1/2) + \mu_{II} (v + 1/2)^2$$

[a]The accuracy of the dipole moments (± 0.001 D) is limited by the uncertainty in the absolute value of the electric Stark field; however, the precision of the results is at least an order of magnitude better (± 0.0001 D).

Table XI. Sodium quadrupole coupling constants for $^{23}Na^{19}F$

$(eqQ)_0 = -8440.1 \pm 1.5$ kc/sec	$(eqQ)_e = -8498.0 \pm 2.6$ kc/sec
$(eqQ)_1 = -8327.9 \pm 1.5$ kc/sec	$(eqQ)_I = +117.0 \pm 4.1$ kc/sec
$(eqQ)_2 = -8220.5 \pm 2$ kc/sec	$(eqQ)_{II} = -2.4 \pm 2.5$ kc/sec

$$(eqQ)_v = (eqQ)_e + (eqQ)_I (v + 1/2) + (eqQ)_{II} (v + 1/2)^2$$

The present hyperfine interaction constants are in agreement with those reported in other electric-resonance studies[21,22] of NaF.

The observed microwave transition frequencies were corrected for Stark and hyperfine splitting by using the dipole moments and hyperfine constants determined in the radio-frequency experiments.

Microwave transitions were observed using Stark fields of both 50 V/cm and 400 V/cm. With the stronger field the uncertainty in the Stark correction is approximately 10 kc/sec whereas with the weaker field this correction is well under 1 kc/sec. Thus, although both results agree well within the experimental error, only the more accurate weak field results are given.

Table XII lists the observed microwave frequencies, the Stark and hyperfine corrections, and the corrected microwave frequencies.

The spectroscopic constants were determined using the familiar Dunham expressions.[27] The vibrational constants, ω_e and $\omega_e x_e$, as given by Ritchie and Lew[28] for NaF were used to calculated D_e and B_e. Table XIII summarizes the spectroscopic constants for $^{23}Na^{19}F$ as determined from the present work and those given by Bauer and Lew.[21]

C. The Radio-Frequency Spectra of $^{39}K^{35}Cl$ and $^{39}K^{37}Cl$

The electric-resonance microwave spectra of KCl were observed previously by Lee et al.[29] and values were reported for the rotational constants, quadrupole coupling constants, and dipole moments. The dipole moments were determined from weak field spectra and exhibited a rather large variation with vibrational state. The present work was therefore undertaken to observe strong field spectra where a more accurate determination of the dipole moment could be made.

From the discussion of Chapter II it follows that in an inhomogeneous electric field the amount of beam deflection is proportional to the product of the effective dipole moment, μ_e, and electric field gradient, $\partial E/\partial x$. A negative effective moment is required in the B field in order to do "flop-in" experiments as discussed previously. From the (1,0) curve in Fig. 2 it

Table XII. Observed microwave transition frequencies and Stark—hyperfine corrections. All transitions were observed at E_c = 50.0 V/cm.

Vibrational State	Line Number	Observed Transition Frequencies (Mc/sec)	J = 0 and J = 1 Stark and Hyperfine Corrections (Mc/sec)	Corrected Transition Frequencies (Mc/sec)
v = 0	II	26062.1602 ± 0.0025	2.6771 ± 0.0005	26059.4831 ± 0.0030
v = 1	II	25791.6142 ± 0.0035	2.6657 ± 0.0005	25688.9485 ± 0.0040
v = 2	II	25523.8680 ± 0.0050	2.6560 ± 0.0006	25521.2120 ± 0.0056

Table XIII. Spectroscopic Constants for $^{23}Na^{19}F$

	Present Results		Bauer and Lew[21]	
D_e ($\sim -Y_{02}$)	0.0347	± 0.0003 Mc/sec	0.0347	± 0.0003 Mc/sec
β_e ($\sim -Y_{12}$)	- 0.00024	± 0.00004 Mc/sec	---	
Y_{01} ($\sim B_e$)	13097.970	± 0.005 Mc/sec	13097.971	± 0.003 Mc/sec
Y_{11} ($\sim -\alpha_e$)	- 136.667	± 0.007 Mc/sec	- 136.665	± 0.004 Mc/sec
Y_{21} ($\sim \gamma_e$)	0.699_5	± 0.004 Mc/sec	0.700	± 0.001 Mc/sec
B_e	13098.029	± 0.060 Mc/sec	13098.032	± 0.035 Mc/sec
B_0	13029.811	± 0.002 Mc/sec	13029.813	± 0.001 Mc/sec[a]
B_1	12894.543	± 0.003 Mc/sec	12894.548	± 0.001 Mc/sec[a]
B_2	12760.674	± 0.004 Mc/sec	12760.683	± 0.001 Mc/sec[a]

$$B_v = Y_{01} + Y_{11}(v + 1/2) + Y_{21}(v + 1/2)^2$$

[a] It is not clear whether the uncertainties given here represent the total expected error or simply the precision of measurement of the observed frequencies.

can be seen that the maximum negative moment is at approximately $\lambda = 2$. This λ value corresponds to a small field and consequently small gradient. The resultant deflection is not as large as the straight-through beam width (~0.005 in.) and therefore sufficient signal intensity can not be obtained with the (1,0) state molecules. However, for the (2,0) state, larger λ values still give a large negative effective moment and sufficient deflection is possible. Therefore J = 1 spectra could not be observed and the observed radio-frequency spectra were produced by transitions of the type $(2, \pm 1) \rightarrow (2,0)$ in the low vibrational states.

The usual commercial tungsten wire exhibits a large potassium noise level. In this experiment use of a specially treated tungsten wire, in which the alkali contamination had been largely removed, reduced the potassium background noise level by a factor of 50 over the commercial wire.

A typical KCl resonance in the v = 0 vibrational state had a full width at half maximum of 20 kc/sec and a signal-to-noise ratio of only 2 to 1. Better statistics of the observed spectra were obtained by computer addition of several runs with a resultant increase in the S/N ratio. Fig. 10 illustrates the effect of adding several spectra of a typical KCl resonance. This technique made possible the analysis of v = 2 spectra, not observable with a single spectral run. The observed and calculated line positions for KCl are listed in Table XIV.

The six major observed resonances of the J = 2 spectrum were due to the potassium quadrupole splitting of the single Stark transition. There was no resolution observable in these six major peaks and therefore additional hyperfine interaction constants could not be determined; however, upper limits on these constants could be set by considering the line widths of the peaks.

Table XV summarizes the present dipole moment determinations and gives comparison with those of Lee et al.[29] There are large differences between the two sets, however the present results now exhibit the expected vibrational variation of the dipole moment.

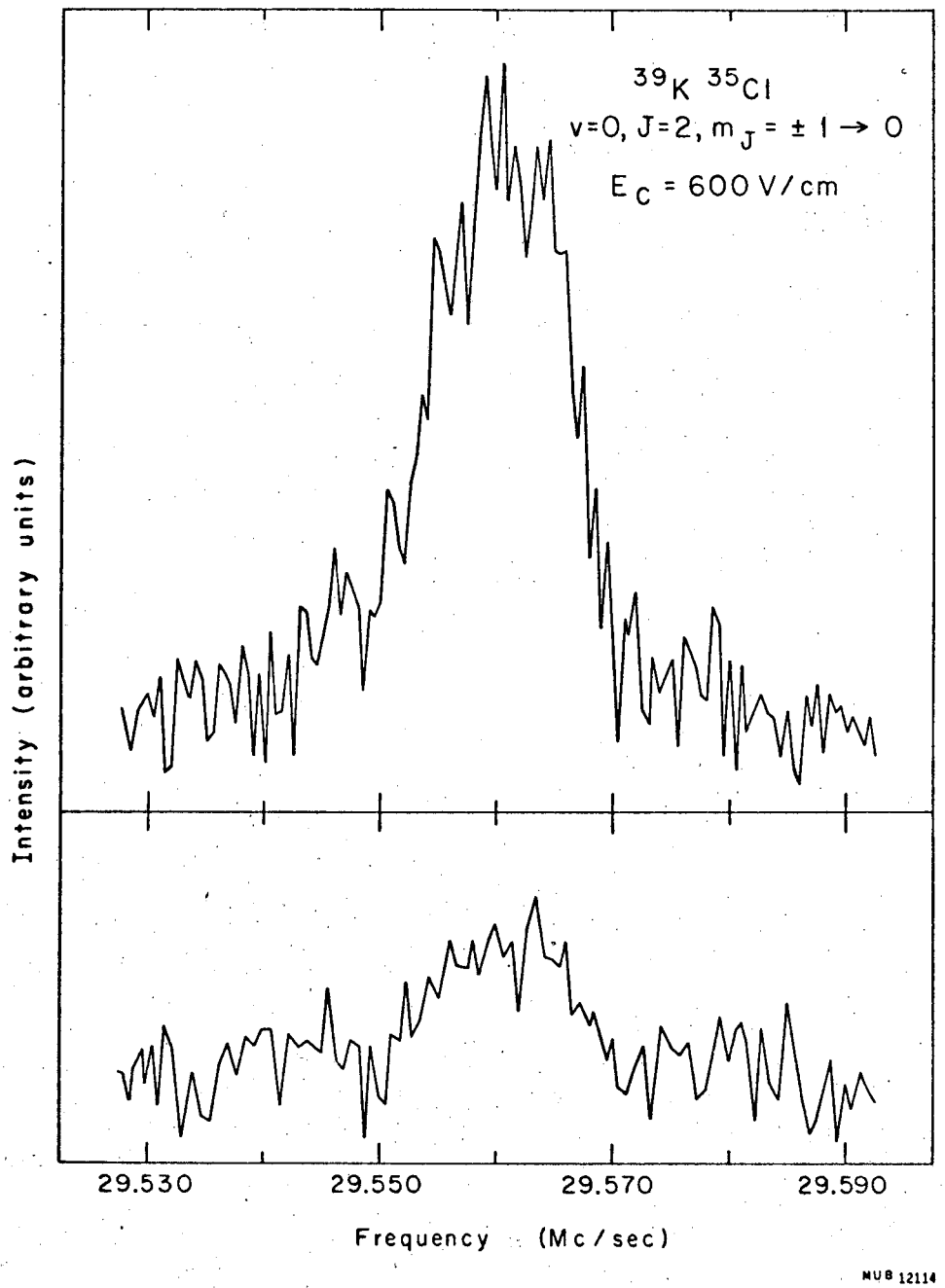

Fig. 10. A typical $^{39}K^{35}Cl$ resonance in the v = 0, J = 1 state. The top figure illustrates the effect of adding ten spectral runs (i.e. bottom figure) of the resonance.

Table XIV. Observed and calculated line positions for the radio-frequency spectra of KCl. All positions are given in kc/sec.

Observed line positions	Calculated line positions	Differences
$^{39}K^{35}Cl$; (2, ±1)→(2,0), v = 0, E_c = 600 V/cm Observed line error is ±1.5 kc/sec.		
29,561.2	29,559.8	-1.4
30,379.2	30,380.4	+1.2
30,481.8	30,483.0	+1.2
30,920.0	30,921.5	+1.5
31,025.2	31,024.0	-1.2
31,845.8	31,844.5	-1.3
$^{39}K^{35}Cl$; (2, ±1)→(2,0), v = 1, E_c = 600 V/cm Observed line error is ±2.5 kc/sec.		
30,140.2	30,142.1	+1.9
30,959.3	30,956.3	-3.0
31,058.0	31,057.8	-0.2
31,490.1	31,493.1	+3.0
31,593.6	31,594.5	+0.9
32,411.5	32,408.7	-2.8
$^{39}K^{35}Cl$; (2, ±1)→(2,0), v = 2, E_c = 600 V/cm Observed line error is ± 4 kc/sec.		
---	30,739	--
31,538	31,538	0
31,640	31,637	-3
32,064	32,065	+1
32,162	32,164	+2
---	32,963	--

Table XIV. (continued)

Observed line positions	Calculated line positions	Differences
$^{39}K^{37}Cl$; $(2, \pm1) \rightarrow (2,0)$, $v = 0$, $E_c = 600$ V/cm Observed line error is ±4 kc/sec.		
---	30,506	--
31,327	31,329	+2
31,431	31,431	0
31,874	31,872	-2
31,972	31,974	+2
---	32,797	--

Table XV. Dipole moments for KCl. All values are given in Debyes.

	Present results	Lee et al.[29]
	$^{39}K^{35}Cl$	
μ_0	10.26875 ± 0.0010	10.48 ± 0.05
μ_1	10.32875 ± 0.0015	
μ_2	10.3877 ± 0.0022	10.69 ± 0.05
μ_e	10.23878 ± 0.0012	
μ_I	0.06000 ± 0.0009	
	$\mu_v = \mu_e + \mu_I(v + 1/2)$	
	$^{39}K^{37}Cl$	
μ_0	10.2683 ± 0.0022	

The potassium quadrupole coupling constants, in good agreement with those reported by Lee et al.,[29] are as follows:

$^{39}K^{35}Cl$: $(eqQ)_0 = -5661 \pm 10$ kc/sec
$(eqQ)_1 = -5615 \pm 20$ kc/sec
$(eqQ)_2 = -5510 \pm 80$ kc/sec

$^{39}K^{37}Cl$: $(eqQ)_0 = -5675 \pm 80$ kc/sec

An upper limit of 200 kc/sec can be placed on the absolute value of the chlorine quadrupole coupling constant for all vibrational states. Also an upper limit of 2 kc/sec can be placed on both spin-rotation interaction constants, c_K and c_{Cl}.

V. A POLARIZABLE ION MODEL OF THE ALKALI HALIDE MOLECULES

A. Introduction

Bonding in the alkali halide molecules is generally assumed to be strongly ionic and this has been the basis of several attempts[30,31,32] to propose a simple ionic model of the alkali halides.

Rittner[33] first used such an ionic model, consisting of polarizable ions, to predict and correlate the dipole moments and dissociation energies of the alkali halides. He assumed that the alkali halide molecule is composed of two ions, each of which is polarized by the electrostatic field of the other. Using the same approach as Debye,[30] who first treated the polarizable ion problem, the total molecular dipole moment can be expressed as:

$$\mu = er-(\mu_1 + \mu_2) \tag{1}$$

Here +e and -e are the charges on the ions; μ_1 and μ_2 are the induced dipole moments, and r is the internuclear separation. Designating the electrostatic field at the center of each ion as E_1 and E_2 and the dipole polarizabilities as α_1 and α_2, the induced moments can be written as:

$$\mu_1 = \alpha_1 E_1 = \alpha_1 \left(\frac{e}{r^2} + \frac{2\mu_2}{r^3} \right) \tag{2}$$

$$\mu_2 = \alpha_2 E_2 = \alpha_2 \left(\frac{e}{r^2} + \frac{2\mu_1}{r^3} \right) \tag{3}$$

Solving these equations simultaneously and substituting into Eq. (1), we obtain:

$$\mu = er-\left(\frac{r^4 e(\alpha_1+\alpha_2) + 4re\alpha_1\alpha_2}{r^6 - 4\alpha_1\alpha_2} \right) \tag{4}$$

Using the crystal lattice theory of Born,[31,32] Rittner expressed the potential energy as:

$$W = \phi + Ae^{-r/\rho} - c/r^6$$

The ϕ term arises from electrostatic interactions between the ions: charge-charge, charge-dipole, and dipole-dipole interactions. This is written as:

$$\phi = -e^2/r - \frac{e^2(\alpha_1+\alpha_2)}{2r^4} - \frac{2e^2\alpha_1\alpha_2}{r^7}$$

The remaining terms of the potential energy are the exponential repulsion term, $Ae^{-r/\rho}$, and Van der Waal's term, $-c/r^6$, where c is a measure of the attractive force between the ions and can be estimated by the method of London.[34]

The repulsion constants, A and ρ, are determined by use of the relationships:

$$\left(\frac{dW}{dr}\right)_{r=r_e} = 0 \qquad (5)$$

$$\left(\frac{d^2W}{dr^2}\right)_{r=r_e} = k \qquad (6)$$

The force constant, k, is related to the vibrational frequency, ν_o, by the relationship:

$$\nu_o = 1/2\pi\sqrt{\frac{k}{\mu_A}}$$

where $\nu_{o/c} = \omega_e$ (the vibrational constant) and μ_A is the reduced mass.

Rittner used Pauling's polarizabilities[35] and experimental spectroscopic constants to calculate the dipole moments, μ, and dissociation energies, W_e, of alkali halides. In general the comparison between Rittner's

predictions and experimental values was good, however the available experimental data was not very complete or accurate, especially in the case of the dipole moments; and a good test of this model could not be made.

Honig et al.[36] extended Rittner's model to predict the Dunham coefficient a_1.[27] The potential energy W(r) can be expanded about r_e and written as:

$$W(r-r_e) = W(r_e) + (r-r_e)\,W'(r_e)^0 + \frac{(r-r_e)^2}{2!}\,W''(r_e) + \frac{(r-r_e)^3}{3!}\,W'''(r_e) + \ldots.$$

or written in the usual Dunham form as:

$$W = W_e + a_o\xi^2 + a_o a_1 \xi^3 + \ldots..$$

where $\xi = \dfrac{r-r_e}{r_e}$ and $a_o = \dfrac{kr_e^2}{2}$

and the second Dunham coefficient is defined as:

$$a_1 = \frac{r_e^3 W'''(r_e)}{3!\,a_o} \qquad (7)$$

The coefficient a_1 can therefore be calculated knowing the form of the potential energy curve and compared to the experimental value:

$$a_1 = \frac{-\alpha_e \omega_e}{6B_e^2} - 1 \qquad (8)$$

Honig et al. found that the agreement was not always good, especially for the lithium halides.

Klemperer et al.,[37,38,39] using more recent experimental data, also examined this model and found that the experimental dipole moment values did not always agree with predictions. They noted that if the polarizabilities apply to a crystal where the ionic fields are relatively low due to symmetry, then they must be adjusted for diatomic molecules where the

fields are higher. Therefore they concluded that the polarizabilities should exhibit a saturation effect in diatomic molecules and derease with field strength. They forced the dipole moments to agree with experimental values by changing the halide polarizabilities and then calculated the values of the dissociation energy, W_e, and the Dunham coefficient, a_1.

Using an inverse powere function, D/r^n, as the form of the repulsion energy, they found the agreement with experimental data not as good as with the usual exponential form, $Ae^{-r/\rho}$.

They also used the model to predict dipole variation with vibrational state, however the available experimental data was so poor that a good comparison with the predicted values could not be made.

Klemperer et al. also considered several forms of the electrostatic term, ϕ, of the potential energy. Using a point charge model, $\phi = -e^2/r$, they found adequate prediction of W_e and a_1, but not of μ. Inclusion of dipole polarizabilities, as in Rittner's model, was required for a dipole moment fit. However consistency required that higher polarizabilities also be included. They therefore used a spherical conductor form of the electrostatic potential which included the higher polarizabilities of the halide ion. The net result was that agreement with observed and calculated values of a_1 was destroyed from the earlier agreement obtained with inclusion of only dipole polarizabilities.

Now with still more experimental data available, re-examination of this model of the alkali halides has again been undertaken with two initial considerations. Klemperer has forced the dipole moments to fit experimental values based on the argument that Pauling's polarizabilities are from a weak field determination and do not apply to the strong field case of the gaseous alkali halides. Cohen,[40,41] however, has shown that the polarizabilities do not necessarily decrease with increasing field strength, as Klemperer has argued. Therefore Klemperer's interpretation of the polarizabilities might not be correct and it is obvious that Pauling's polarizabilities do not give a good prediction of dipole moments. For this reason it seems warranted to give further study to the polarizabilities.

Also, as Klemperer noted, the model in order to be consistent must include contributions from higher electrostatic interactions between the ions, that is charge-multipole and multipole-multiple terms. The present work therefore approaches the problem by including several effects, previously neglected, in an effort to obtain a consistent model for predicting the values of the dissociation energy, W_e, the Dunham coefficient, a_1, and the dipole moment, μ, of the alkali halide molecules.

B. The Polarizabilities

Recently Bruns[42] has calculated the dipole, quadrupole, octupole, and hexadecapole polarizabilities in order to determine the antishielding factors for an interpretation of the quadrupole coupling constants in the alkali halides. The polarizabilities were calculated for the alkali halide internuclear distances and were often much smaller than those for the free ion. These polarizabilities also exhibited a variation with internuclear separation, that is they increased with increasing r. These results seem consistent since it would be expected that the polarizability should decrease with charge penetration. At alkali halide internuclear distances the positive alkali core penetrates the electron density of the large halide ion, but the electron density is penetrated only for a few of the alkali ions, and thus this penetration effect is primarily important in the case of the halide polarizabilities.

It seems reasonable to expect the polarizabilities to fit a curve varying from zero at $r = 0$ to the free ion value at some finite r value, R. This R value, approximating the limit of the electron distribution contributing to the polarizability, should be larger for higher polarizabilities since the contribution from the outer part of the electron distribution becomes much larger for the higher polarizabilities.

Using the variation of parameters method Bruns calculated the polarizabilities for the F^- and Cl^- ions at several values of r. He assumed a cancellation of the $p \rightarrow s$ and $s \rightarrow p$ contributions to the dipole calculation. However, Sternheimer[43] has shown that these terms do not cancel in the case

of the halides. The higher polarizability calculations of Burns include contributions from all terms and should indicate the behavior of these polarizabilities, at least in the case of the alkali halides.

In analyzing Burns' results it can be seen that the slope of the polarizability curve increases and the curve is displaced to higher r values as one goes to higher polarizabilities. Therefore one would like to propose a simple variation of the polarizability with internuclear seperation, r, which would satisfy these conditions. Burns' data for the F^- and Cl^- ions can be fitted to curves of the form:

$$\alpha_i^n = \alpha_i^n(\text{free ion}) \sin^{2n}\left(\frac{r}{\frac{(3+n)}{2} r_o}\right) \qquad (9)$$

Here α_i^n is the polarizability at r where n = 1,2,.... represents the dipole, quadrupole,....polarizabilities. The crystal radii, r_o, of Pauling[44] give a reasonable representation of the variation of electron distribution as a function of the ion. Several approaches have been used in calculating free ion polarizabilities, $\alpha_i^n(\text{free ion})$, and for the present calculations a consistent set[45] of dipole polarizabilities, obtained from a semi-emperical extrapolation of the polarizabilities of the positive ions (estimated from spectroscopic data) and the measured polarizabilities of the rare gases, has been used for the halide ions. This set is:

ion	$\alpha_H^n(\text{free ion})(\text{Å})^3$
F^-	1.70
Cl^-	5.04
Br^-	6.90
I^-	10.50

Pauling's polarizabilities[35] are used for the alkali free ion value. At the lithium halide internuclear distances the above halide set gives dipole polarizabilities which are quite close to Pauling's halide values, but for

the other alkali halide distances they are considerably larger. The higher free ion polarizabilities, calculated from the dipole ion values, using a spherical conductor model, are given as:

$$\alpha_i^n(\text{free ion}) = \frac{a^{2n+1}}{n!} \tag{10}$$

where a is the radius of the spherical conductor.

Burns' values for the octupole and hexadecapole polarizabilities are somewhat higher than what Eq. (9), using the above set of halide polarizabilities, would predict. It should be pointed out that the calculation of the higher polarizabilities must treat the problem accurately for large r, and Hartree-Fock wave functions may over-estimate the contribution of terms at large r and thus give polarizabilities too large.

Although the proposed polarizability function is at best, a good guess, it does adequately fit the available data for the alkali halides. This function seems to represent a reasonable variation with r and calculations have even shown that the potential energy function is quite insensitive to the exact form of the polarizability function at alkali halide internuclear distances, especially in the case of the higher polarizabilities.

C. The Potential Energy

The general form of the potential energy function:

$$W = \phi_E + \phi_R - c/r^6 \tag{11}$$

contains an electrostatic term, ϕ_E, a repulsion term, ϕ_R, and Van der Waal's term, $-c/r^6$.

The ϕ_E term arises from electrostatic interactions between the ions and, as previously noted, consistency requires the inclusion of contributions from all multipole terms. This has therefore been the approach of the present treatment of the electrostatic term.

If we consider the alkali halide molecule of two polarizable ions with a positive charge at ion A and a negative charge at ion H with H-A the z direction, the general form of the potential at site H due to an induced 2^ℓ moment at site A is:[46]

$$v = \frac{p_A^{(\ell)} P_\ell(\cos\theta)}{r^{\ell+1}} = (-1)^\ell p_A(\ell) \frac{\partial^\ell}{\partial z^\ell}\left(\frac{1}{r}\right)$$

where $p_A^{(\ell)}$ is the induced moment and θ the angle between z and r. We can then write the total potential (including the contribution from the charge at site A) as:

$$V_H = -\frac{e}{r} + \sum_{\ell=1} \frac{p^{(\ell)}}{r^{\ell+1}}$$

and therefore the field at site H can be written:

$$E_H = -\partial V_H/\partial r = -\frac{e}{r^2} + \sum_{\ell=1} \frac{(\ell+1)p_H^{(\ell)}}{r^{\ell+2}}$$

If we consider an induced moment $p_H^{(m)}$ at H in the electric field E_H, the force f on the moment can be written:

$$f = \frac{p_H^{(m)}}{m!} \frac{\partial^m E_A}{\partial r^m}$$

and the total force F on ion H is given:

$$F = \frac{e^2}{r^2} - e\left(\sum_{\ell=1} \frac{p_A^{(\ell)}(\ell+1)}{r^{\ell+2}} + \sum_{m=1} \frac{p_H^{(\ell)}(m+1)}{r^{m+2}}\right) + \sum_{\ell=1} \sum_{m=1} \frac{p_A^{(\ell)} p_H^{(m)}}{r^{\ell+m+2}} \frac{(\ell+m+1)!}{\ell!\, m!} \qquad (12)$$

The polarizability, α_i^ℓ, is defined from:

$$p_A^{(\ell)} = (-1)^\ell \alpha_A{}^\ell \frac{\partial^{\ell-1} E_A}{\partial_r{}^{\ell-1}} \qquad (13)$$

where $p_A^{(\ell)}$ is the induced moment and E_A is the field at site A. The moments can be written in the expanded form as:

$$p_A^{(\ell)} = \alpha_A^{\ell} - \frac{e\ell!}{r^{\ell+1}} + \sum_{m=1} \frac{p_H^{(m)}}{r^{m+\ell+1}} \frac{(m+\ell)!}{m!} \tag{14}$$

$$p_H^{(\ell)} = \alpha_H^{\ell} - \frac{em!}{r^{m+1}} + \sum_{\ell=1} \frac{p_A^{(\ell)}}{r^{m+\ell+1}} \frac{(m+\ell)!}{\ell!} \tag{15}$$

and these equations are solved simultaneously.

The total electrostatic potential energy between ions is therefore:

$$\phi_E = \int_{\infty}^{r_e} F = -\frac{e^2}{r_e} - \int_{\infty}^{r_e} e \left(\sum_{\ell=1} \frac{p_A^{(\ell)}(\ell+1)}{r^{\ell+2}} + \sum_{m=1} \frac{p_H^{(\ell)}(m+1)}{r^{m+2}} \right) + \int_{\infty}^{r_e} \sum_{\ell=1} \sum_{m=1} \frac{p_A^{(\ell)} p_H^{(m)}}{r^{\ell+m+2}} \frac{(\ell+m+1)!}{\ell!\, m!} \tag{16}$$

where the terms represent the charge-charge, charge-multipole, and multipole-multipole interactions, respectively. The ϕ_E term is calculated using the polarizabilities, as discussed in the previous section, and experimental internuclear distances, r_e.

Previously, both the exponential, $Ae^{-r/\rho}$, and inverse power, D/r^n, forms had been used to represent the repulsion interaction. An accurate representation undoubtedly requires a considerably more complicated function. In the only well-studied case[47] (repulsion between two helium atoms), the interaction form is a polynomial in r and $1/r$ times an exponential function of r. The present treatment therefore uses a best single term representation of the form, $Ar^n e^{-r/\rho}$, where n is given the same value for all alkali halides. This repulsion term allows more flexibility in fitting the model to experimental values of W_e and a_1. Here A and ρ are calculated through use of Eq. (5) and (6).

Van der Waal's attractive force constant c is estimated as:[34]

$$c = \frac{3}{2}\alpha_A^1\alpha_H^1 \frac{I_A^{(II)}(-E_H')}{I_A^{(II)} - E_H'} \qquad (17)$$

where α_A^1 and α_H^1 are the dipole polarizabilities of the ions, $I_A^{(II)}$ is the second ionization potential[48] of the alkali atom and E_H' is the electron affinity[49] of the halogen atom.

The dissociation energy W_e can therefore be calculated from Eq. (11) and compared to the experimental value:

$$W_e = D_o + I_A^{(I)} - E_H' + 1/2h\nu_o \qquad (18)$$

where D_o is the dissociation energy[50] into neutral atoms, $I_A^{(I)}$ is the first ionization potential[48] of the alkali atom, E_H' is the electron affinity[49] of the halogen atom, and $1/2h\nu_o$ is the correction for zero point vibrational energy.

Table XVI shows the comparison between calculated and experimental values of W_e with a best fit obtained using $n = -2$ in the repulsion term. Inclusion of higher multipole field terms in the calculation of the moments with Eq. (14) and (15) leads to complicated integrals of Eq. (16). Therefore in the calculation of ϕ_E (but not the derivatives) the approximation has been made that multipole field terms higher than the dipole do not contribute appreciably to the moments. It is estimated that this approximation gives a low value of ϕ_E in CsI (the most severe case) by less than 0.2 ev.

The values of the Dunham coefficient a_1 are calculated using the third derivative of the potential energy function, Eq. (7), and are compared in Table XVI with the experimental values, Eq. (8), calculated from spectroscopic constants.

The agreement of the calculated and experimental values of W_e and a_1 is quite good for the alkali halides with small alkali ions, but not as good when both ions are rather large. The proper treatment of the multipole-

Table XVI. The calculated and experimental values of W_e and a_1 for the alkali halide molecules

	W_e(calc.)	W_e(expt.)[a]	a_1(calc.)	a_1(expt.)
LiF	-7.893	-7.930	-2.520	-2.701[b,c]
LiCl	-6.462	-6.560	-2.633	-2.721[d,e]
LiBr	-6.115	-6.380	-2.705	-2.718[f,g,h]
LiI	-5.702	-5.990	-2.743	-2.730[f,h,i]
NaF	-6.590	-6.640	-2.921	-3.133[j,k,l]
NaCl	-5.597	-5.650	-3.002	-3.076[m]
NaBr	-5.345	-5.530	-2.973	-3.046[f]
NaI	-5.034	-5.220	-2.977	-3.016[f]
KF	-5.785	-5.990	-3.224	-3.116[n]
KCl	-4.901	-5.040	-3.301	-3.226[m]
KBr	-4.679	-4.890	-3.306	-3.242[f,o]
KI	-4.407	-4.580	-3.307	-3.246[f]
RbF	-5.707	-5.770	-3.359	-3.135[n]
RbCl	-4.651	-4.810	-3.668	-3.297[m]
RbBr	-4.450	-4.720	-3.692	-3.326[f]
RbI	-4.189	-4.430	-3.514	-3.344[f]
CsF	-5.716	-5.640	-3.507	-3.032[n]
CsCl	-4.522	-4.770	-4.003	-3.319[m]
CsBr	-4.187	-4.710	-4.081	-3.377[f]
CsI	-3.951	-4.410	-3.853	-3.429[f]

[a] Ref. 50
[b] Ref. 51
[c] Ref. 52
[d] Ref. 53
[e] Ref. 54
[f] Ref. 55
[g] Ref. 56
[h] Ref. 57
[i] Ref. 58
[j] Ref. 21
[k] Ref. 24
[l] Ref. 28
[m] Ref. 59
[n] Ref. 60
[o] Ref. 61

multipole terms is particularly important for the case of two large polarizable ions and this suggests that possibly the spherical conductor approximation of the higher free ion polarizabilities is not quite correct. It is also quite probable that the form of the repulsion term $Ar^n e^{-r/\rho}$ is an over-simplification, and here again the most serious defect would be expected for the case of two large polarizable ions. The important feature of this model, however, is that all higher electrostatic interactions have been included without destroying the agreement between calculated and experimental values of W_e and a_1.

D. The Dipole Moment

Using the same approach as Debye[30] had done for the hydrogen halides, Rittner[33] represented the polarizable ion model of the alkali halide molecule as:

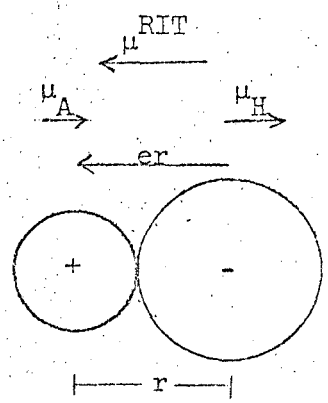

where μ_A and μ_H are the alkali and halide induced dipole moments and the net molecular dipole moment is:

$$\mu^{RIT} = er - \mu_A - \mu_H \tag{19}$$

Eq. (19) is then written in the usual form:

$$\mu^{RIT} = er - \left(\frac{r^4 e(\alpha_A^1 + \alpha_H^1) + 4re\,\alpha_A^1\alpha_H^1}{r^6 - 4\alpha_A^1\alpha_H^1} \right) \tag{20}$$

Recent experimental dipole moment data have been fitted to expressions of the form:

$$\mu_v = \mu_e + \mu_I (v + 1/2) \tag{21}$$

where μ_e is the equilibrium dipole moment and μ_I represents the vibrational variation of the moment. Therefore comparison of experimental and calculated μ_I values should serve as a further test of the model.

If we let $\xi = \dfrac{r-r_e}{r_e}$, μ can be expanded in the form:

$$\mu = \mu_e + \left(\frac{d\mu}{d\xi}\right)_{\xi=0} \xi + 1/2 \left(\frac{d^2\mu}{d\xi^2}\right)_{\xi=0} \xi^2 + \ldots\ldots \tag{22}$$

and the average value over vibrational state written as:

$$\langle\mu\rangle_v = \mu_e + \left(\frac{d\mu}{d\xi}\right)_{\xi=0} \langle\xi\rangle_v + 1/2 \left(\frac{d^2\mu}{d\xi^2}\right)_{\xi=0} \langle\xi^2\rangle_v + \ldots\ldots \tag{23}$$

For an anharmonic oscillator we can approximate:

$$\langle\xi\rangle_v = -3a_1 \frac{B_e}{\omega_e} (v + 1/2) \tag{24}$$

$$\langle\xi^2\rangle_v = 2\frac{B_e}{\omega_e} (v + 1/2) \tag{25}$$

and therefore write:

$$\langle\mu\rangle_v = \mu_e + \left[-3a_1 \frac{B_e}{\omega_e} \left(\frac{d\mu}{d\xi}\right)_{\xi=0} + \frac{B_e}{\omega_e} \left(\frac{d^2\mu}{d\xi^2}\right)_{\xi=0} \right] (v + 1/2) \tag{26}$$

The quantity in brackets is the calculated μ_I term and can be compared to the experimental μ_I term in Eq. (21).

Table XVII compares μ_e^{RIT} and μ_I^{RIT} with experimental μ_e and μ_I values. It can be seen that the agreement is very poor; the Rittner dipole function predicts low μ_e values and μ_I values too large.

Looking again at the polarizable ion model, it can be seen that the Debye molecular dipole moment neglects dipolar effects associated with repulsion, and although this is correct for the case of the hydrogen halides, it is not for the alkali halides.

If we consider the repulsion force (in the z direction) on the halide ion, it can be approximated as:

$$f = - E_h q_h \qquad (27)$$

where E_h is the field at the closed core of charge $q_h = +7e$ (the halide ion minus the eight outer electrons). This field E_h arises from changes (due to the repulsion interaction) in the outer electron distribution of the halide ion and from the repulsion induced moments at the alkali ion.

If we consider the outer electrons on the halide ion, the repulsion effect gives a charge density that changes:

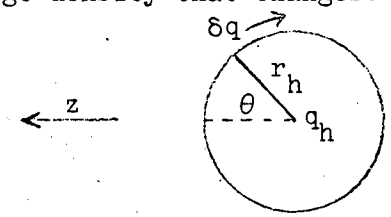

and therefore:

$$\delta E = \frac{\delta q \cos\theta}{r_h^2}$$

where r_h is the distance of charge q from the core. We can then write:

$$\delta\mu = \delta q \, r_h \cos\theta$$

$$\frac{\delta\mu}{\delta E} = r_h^3$$

$$\mu_h = R_h^3 E_h^e$$

Table XVII. The calculated and experimental dipole moments of the alkali halide molecules.

	μ_e^{RIT}	μ_e^{REP}	μ_e(calc.)	μ_e(expt.)	μ_I^{RIT}	μ_I^{REP}	μ_I(calc.)	μ_I(expt.)
LiF	5.272	1.021	6.292	6.284[a]	.096	-.0182	.077	.082[a]
LiCl	5.365	1.616	6.981	7.085[b]	.104	-.0245	.079	.081[b]
LiBr	5.340	1.836	7.176	7.226[c]	.103	-.0253	.077	.077[c]
LiI	5.217	2.185	7.403	7.387[d]	.106	-.0279	.078	.078[d]
NaF	6.992	1.106	8.098	8.123[e]	.076	-.0169	.059	.064[e]
NaCl	7.214	1.731	8.946	8.970[f]	.074	-.0203	.054	.061[f]
NaBr	7.178	1.957	9.135		.067	-.0189	.048	
NaI	7.039	2.308	9.347		.066	-.0199	.046	
KF	7.450	1.105	8.555	8.550[g]	.080	-.0169	.063	.069[g]
KCl	8.270	1.972	10.242	10.239[a]	.076	-.0225	.053	.060[a]
KBr	8.381	2.252	10.633		.065	-.0208	.044	
KI	8.446	2.659	11.105		.063	-.0215	.041	
RbF	7.429	1.025	8.454	8.514[h]	.077	-.0147	.063	.067[h]
RbCl	8.433	2.086	10.519		.074	-.0239	.050	
RbBr	8.582	2.431	11.013		.059	-.0211	.038	
RbI	8.722	2.910	11.632		.053	-.0195	.033	
CsF	6.922	.869	7.791	7.849[i]	.082	-.0127	.069	.070[i]
CsCl	8.284	2.224	10.508	10.415[j]	.080	-.0273	.053	
CsBr	8.485	2.689	11.174		.063	-.0246	.038	
CsI	8.732	3.316	12.048		.054	-.0223	.032	

[a] present work [d] Ref. 58 [g] Ref. 62 [j] Ref. 65
[b] Ref. 54 [e] Ref. 24 [h] Ref. 63
[c] Ref. 56 [f] Ref. 15 [i] Ref. 64

where μ_n is the repulsion induced dipole moment of the halide ion. The field at the core, E_h^e, arises from the changing halide electron distribution at an average distance R_h from the core. Similarly for the alkali ion we have a repulsion moment in the opposite direction:

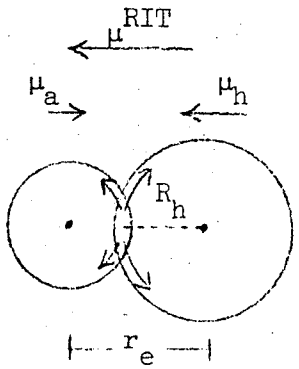

In the alkali halide molecule the electron distribution of the highly polarizable halide ion is favored between the ions, but for the alkali ion, which is not very polarizable, the electron distribution is directed out of the region of the halide ion, and thus a more accurate picture of the molecule would be:

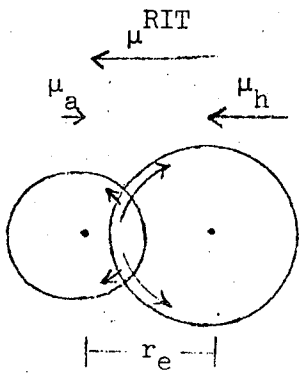

It would therefore be expected that the repulsion effect would cause a changing electron distribution mostly on the halide ion, and in the present treatment the field is evaluated at the halide core. This field E_h is due to a change in the outer electron distribution at H, E_H^e, and the field associated with the small repulsion dipole moment μ_a at A. The field arising from other repulsion moments at A is small and has been neglected. The total field can therefore be written as:

$$E_h = \frac{\mu_h}{R_h^3} - \frac{2\mu_a}{r_e^3} \tag{28}$$

The average distance R_h of the changing electron distribution (in the ion-ion overlap area) should be a function of the distance from the halide core to the alkali ion and this has been approximated as $R_h = \gamma r_e$ where γ is a scaling factor of r_e, the internuclear distance. The repulsion moments should approximately be a function of their respective polarizabiliites. However, because the repulsion effect should be weighted heavily on the halide ion, as discussed above, the repulsion induced moment μ_a should be proportionally smaller than μ_h. This has been expressed as:

$$\frac{\mu_a}{\mu_h} = \beta \frac{\alpha_A^1}{\alpha_H^1} \tag{29}$$

The net repulsion dipole moment is therefore:

$$\mu^{REP} = \mu_h - \mu_a = \frac{f}{q_h} \gamma^3 r_e^3 \frac{\left(1-\beta\frac{\alpha_A^1}{\alpha_H^1}\right)}{\left(1+2\,\gamma^3\beta\frac{\alpha_A^1}{\alpha_H^1}\right)} \tag{30}$$

We can now write the total equilibrium molecular dipole moment as:

$$\mu_e = \mu_e^{RIT} + \mu_e^{REP} \tag{31}$$

and the vibrational variation coefficient as:

$$\mu_I = \mu_I^{RIT} + \mu_I^{REP} \tag{32}$$

A best fit of the dipole moments has been obtained when $\gamma = 0.81$ and $\beta = 0.40$ (for all alkali halides) and Table XVII lists the μ_e^{REP} and μ_I^{REP} values. This table then compares the total calculated dipole moments, μ_e and μ_I, with experimental values and the agreement is extremely good.

The treatment of the repulsion moment undoubtedly neglects some effects. For example, the average distance R_h to the overlap should take into consideration the particular ions of the molecule and not simply be a scaled r_e. Even so, this simple treatment of the dipole moment has allowed a very good fit with all experimental μ_e and μ_I values of the alkali halides.

E. Concluding Remarks

The approach of the polarizable ion model presented here has been to include several effects, previously neglected. These include the treatment of the polarizability as a function of r, inclusion of all multipole terms, and consideration of a repulsion dipole moment. The net result has been that this semi-classical model removes the inconsistencies of earlier treatments and successfully gives a good fit of the potential energy and dipole moment functions with the experimental data of the alkali halides.

As a further verification of this model, one would like to make an extension to other ionic molecules, i.e. the hydrogen halides. Undoubtedly the present model makes over-simplifications of some terms such as the repulsion energy and the polarizability function. And, although these terms adequately fit the alkali halides, they may not be the general form for other molecules. Therefore a more complete theoretical study is probably required before this model can be extended beyond the alkali halides.

ACKNOWLEDGEMENTS

I would like to thank Professor Kenneth Street, Jr. for his encouragement and helpful guidance throughout the course of this work.

The advice and assistance of Dr. Alvin J. Hebert is also greatly appreciated. Thanks are due to the other members of the molecular-beam group for their assistance and helpful discussions.

This work was performed under the auspices of the U. S. Atomic Energy Commission.

REFERENCES

1. H. K. Hughes, Phys. Rev 72, 614 (1947).
2. R. O. Carlson, C. A. Lee and B. P. Fabricand, Phys. Rev. 85, 784 (1952).
3. L. Wharton, W. Klemperer, L. P. Gold, R. Strauch, I. I. Gallagher and V. E. Derr, J. Chem. Phys. 38, 1203 (1963).
4. J. C. Swartz and J. W. Trischka, Phys. Rev. 88, 1085 (1952).
5. R. G. Luce and J. W. Trischka, J. Chem. Phys. 21, 105 (1953).
6. R. Braunstein and J. W. Trischka, Phys. Rev. 98, 1095 (1955).
7. A. J. Hebert, A Molecular-Beam Electric-Resonance Spectrometer and the Radio-Frequency Spectra of Lithium Fluoride (Ph. D. Thesis), UCRL-10482, Sept. 1962.
8. N. F. Ramsey, Molecular Beams (Clarendon Press, Oxford, 1956).
9. G. Gräff, W. Paul, and Ch. Schlier, Z. Physik 153, 38 (1958).
10. N. F. Ramsey, Phys. Rev. 91, 303 (1953).
11. Reference 10, p. 230.
12. F. W. Breivogel, The Radio-Frequency and Microwave Spectra of LiBr and LiI. (Ph. D. Thesis), UCRL-11665, Sept. 1964.
13. V. Fano, J. Res. Natl. Bur. Standards 40, 215 (1948).
14. S. O. Kastner, A. M. Russell and J. W. Trischka, J. Chem. Phys. 23, 1730 (1955).
15. L. P. Gold, The Molecular Beam Electric Resonance Spectra of Some Alkali Halides (Ph. D. Thesis), Harvard University, Cambridge, Mass., Nov. 1961.
16. L. Wharton, L. P. Gold and W. Klemperer, Phys. Rev. 133, B270 (1964).
17. L. Wharton and W. Klemperer, J. Chem. Phys. 39, 1881 (1963).
18. N. G. Cranna, Can. J. Phys. 31, 1185 (1953).
19. N. A. Schuster and G. E. Pake, Phys. Rev. 81, 157 (1951).
20. R. L. White, Rev. Mod. Phys. 27, 276 (1955).
21. R. K. Bauer and H. Lew, Can. J. Phys. 41, 1461 (1963); 42, 830 (1964).
22. G. Gräff and G. Werth, Z. Physik 183, 223 (1965).
23. S. E. Veazey and W. Gordy, Phys. Rev. 138, A1303 (1965).
24. C. D. Hollowell, A. J. Hebert and K. Street, Jr. J. Chem. Phys. 41, 3540 (1964).

25. H. J. Zeiger and D. I. Bolef, Phys. Rev. 85, 788 (1952).
26. R. A. Logan, R. E. Cote and P. Kusch, Phys. Rev. 86, 280 (1952).
27. J. L. Dunham, Phys. Rev. 41, 721 (1932).
28. R. K. Ritchie and H. Lew, Can J. Phys. 42, 43 (1964).
29. C. A. Lee, B. P. Fabricand, R. O. Carlson and I. I. Rabi, Phys. Rev. 91, 1395 (1953).
30. P. Debye, Polar Molecules (Dover Publications, New York, 1945).
31. M. Born and W. Heisenberg, Z. Physik 23, 388 (1924).
32. M. Born and J. E. Mayer, Z. Physik 75, 1 (1932).
33. E. S. Rittner, J. Chem. Phys. 19, 1030 (1951).
34. F. London, Z. Physik 63, 245 (1930).
35. L. Pauling, Proc Roy. Soc. (London) A114, 191 (1927).
36. A. Honig, M. Mandel, M. L. Stitch, and C. H. Townes, Phys. Rev. 96, 629 (1954).
37. W. Klemperer and S. A. Rice, J. Chem. Phys. 26, 618 (1957).
38. S. A. Rice and W. Klemperer, J. Chem. Phys. 27, 573 (1957).
39. W. Klemperer, W. G. Norris, and A. Büchler, J. Chem. Phys. 33, 1534 (1960).
40. H. D. Cohen, J. Chem. Phys. 43, 3558 (1965).
41. H. D. Cohen, J. Chem. Phys. 45, 10 (1966).
42. G. Burns, Phys. Rev. 115, 357 (1959).
43. R. M. Sternheimer, Phys. Rev. 115, 1198 (1959).
44. Linus Pauling, The Nature of the Chemical Bond (Cornell University Press, Ithaca, New York, 1960) p. 526.
45. K. Street, Jr. (University of California, Berkeley), private communication, September 1966.
46. W. K. Panofsky and M. Phillips, Classical Electricity and Magnetism (Addison-Wesley Publishing Company, Inc., Reading, Mass., 1962).
47. J. Slater, Quantum Theory of Molecules and Solids, Vol. 1, (McGraw-Hill Book Company, Inc., New York, 1963).
48. C. E. Moore, U. S. Nat. Bur. of Standards Circ. No. 467, Vol. 1 (1949), Vol. 2 (1952), Vol. 3 (1958).
49. R. S. Berry and C. W. Reimann, J. Chem. Phys. 38, 1540 (1963).

50. Leo Brewer, The Thermodynamic Properties of the Alkali Halides, UCRL-9952, November 1961.

51. L. Wharton, W. Klemperer, L. P. Gold, R. Strauch, J. J. Gallagher and V. E. Derr, J. Chem. Phys. 38, 1203 (1963).

52. G. L. Vidale, J. Phys. Chem. 64, 314 (1960).

53. D. R. Lide, Jr., P. Cahill and L. P. Gold, J. Chem. Phys. 40, 156 (1964).

54. Troy Story (University of California, Berkeley), private communication, October 1966.

55. J. R. Rusk and W. Gordy, Phys. Rev. 127, 817 (1962).

56. A. J. Hebert, F. W. Breivogel, Jr. and K. Street, Jr., J. Chem. Phys. 41, 2368 (1964).

57. W. Klemperer, W. G. Norris, A. Büchler and A. G. Emslie, J. Chem. Phys. 33. 1534 (1961).

58. F. W. Breivogel, Jr., A. J. Hebert and K. Street, Jr., J. Chem. Phys. 42, 1555 (1965).

59. P. L. Clouser and W. Gordy, Phys. Rev. 134, A863 (1964).

60. S. E. Veazey and W. Gordy, Phys. Rev. 138, A1303 (1965).

61. B. P. Fabricand, R. O. Carlson, C. A. Lee and I. I. Rabi, Phys. Rev. 91, 1403 (1953).

62. G. Gräff and O. Runolfsson, Z. Physik 176, 90 (1963).

63. Frank Lovas (University of California, Berkeley), private communication, September, 1966.

64. Frank Lovas (University of California, Berkeley), private communication, November, 1966.

65. R. G. Luce and J. W. Trischka, J. Chem. Phys. 21, 105 (1953).